ČESKÉ VYSOKÉ
UČENÍ TECHNICKÉ
V PRAZE

FAKULTA ELEKTROTECHNICKÁ

BAKALÁŘSKÁ PRÁCE

2023

JOSEF
HAVLAS

České vysoké učení technické v Praze

Fakulta elektrotechnická

Katedra teorie obvodů

Bakalářská práce

Metody pro získání věrohodných fázových zpoždění otoakustických emisí

Methods for obtaining reliable phase-gradient delays from otoacoustic emission data

Autor: Josef Havlas

Vedoucí práce: Ing. Václav Vencovský, Ph.D.

Studijní program: Lékařská elektronika a bioinformatika

Praha 2023

ZADÁNÍ BAKALÁŘSKÉ PRÁCE

I. OSOBNÍ A STUDIJNÍ ÚDAJE

Příjmení: **Havlas** Jméno: **Josef** Osobní číslo: **499112**

Fakulta/ústav: **Fakulta elektrotechnická**

Zadávající katedra/ústav: **Katedra teorie obvodů**

Studijní program: **Lékařská elektronika a bioinformatika**

II. ÚDAJE K BAKALÁŘSKÉ PRÁCI

Název bakalářské práce:

Metody pro získání věrohodných fázových zpoždění otoakustických emisí

Název bakalářské práce anglicky:

Methods for obtaining reliable phase-gradient delays from otoacoustic emission data

Pokyny pro vypracování:

Fázové zpoždění otoakustických emisí (OAE) v lidském uchu by mělo odpovídat skupinovému zpoždění kochleárních filtrů. Proto je možno využít OAE pro neinvazivní měření zpoždění kochleárních filtrů, které je spojeno s šířkou pásma těchto filtrů. Interpretace fázového zpoždění OAE je poněkud složitá kvůli velkému kolísání emisí samotných, pro odhad tohoto zpoždění je známo mnoho různých metod. Implementujte vybrané metody a vyhodnoťte je na OAE evokovaných čistým tónem (SFOAE) a OAE evokovaných transientním signálem (TEOAE) získaných z nelineárního kochleárního modelu a naměřených v lidském uchu.

Seznam doporučené literatury:

Shera, C.A. & Bergevin, C. (2012) Obtaining reliable phase-gradient delays from otoacoustic emission data. J. Acoust. Soc. Am. 132, 927-943. doi: 10.1121/1.4730916

Jméno a pracoviště vedoucí(ho) bakalářské práce:

Ing. Václav Vencovský, Ph.D. katedra radioelektroniky FEL

Jméno a pracoviště druhé(ho) vedoucí(ho) nebo konzultanta(ky) bakalářské práce:

Datum zadání bakalářské práce: **14.12.2022** Termín odevzdání bakalářské práce: _____

Platnost zadání bakalářské práce: **24.09.2024**

Ing. Václav Vencovský, Ph.D.	doc. Ing. Radoslav Bortel, Ph.D.	prof. Mgr. Petr Páta, Ph.D.
podpis vedoucí(ho) práce	podpis vedoucí(ho) ústavu/katedry	podpis děkana(ky)

III. PŘEVZETÍ ZADÁNÍ

Student bere na vědomí, že je povinen vypracovat bakalářskou práci samostatně, bez cizí pomoci, s výjimkou poskytnutých konzultací. Seznam použité literatury, jiných pramenů a jmen konzultantů je třeba uvést v bakalářské práci.

. _____ Datum převzetí zadání

_____ Podpis studenta

Prohlášení

Prohlašuji, že jsem předloženou práci vypracoval samostatně a že jsem uvedl veškeré použité informační zdroje v souladu s Metodickým pokynem o dodržování etických principů při přípravě vysokoškolských závěrečných prací.

V Praze dne 26.5.2023 .....

Podpis autora práce

Poděkování

Předně bych chtěl poděkovat panu Ing. Václavu Vencovskému, Ph.D. za odborný dohled nad psaním této práce. Také bych mu rád poděkoval za ohromnou podporu a trpělivost ve chvílích, kdy jsem si nevěděl rady a potřeboval pomoct s dalším postupem. Dále bych rád poděkoval mému supervizorovi na zahraniční stáži v kanadském Montréalu, panu M. ing Christianu Cardinalovi, Ph.D., který taktéž obohatil tuto bakalářskou práci. Práce vznikla v rámci projektu č. 23-07621J Grantové agentury České republiky.

Abstrakt

Otoakustické emise (OAE) jsou akustické vlny naměřené ve zvukovodu, které jsou generovány uchem. Tyto emise jsou využívány při klinických vyšetřeních sluchu. Jejich absence signalizuje problém se sluchem, který je posléze hlouběji analyzován. Otoakustické emise mohou sloužit nejen jako nástroj při vyšetření, ale také pro objektivní stanovení charakteristik sluchové periferie. Například latence otoakustických emisí způsobených odrazem nám poskytuje nepřímý nástroj pro měření naladění kochleárních filtrů. Tato práce uvádí a ověřuje dvě metody pro získání věrohodných zpoždění OAE, které byly vyvinuty Sherou a Bergevinem (2012): algoritmus výběrů maxim a metoda kepstrální analýzy. Shera a Bergevin (2012) ověřili tyto metody použitím simulovaných OAE odvozených z lineárního modelu kochley. Zde využíváme naopak nelineárního kochleárního modelu, který nám dovoluje studovat závislost latence OAE na úrovni vyvolávajícího stimulu. Pro simulované emise jsou výsledky při srovnání s odhadovanými referenčními hodnotami poměrně přesné. Metody byly aplikovány i na experimentálně aplikovaná data, která potvrdila validitu použitého modelu emisí.

Klíčová slova: otoakustické emise, fázové zpoždění, vyhlazení fáze, kochleární filtry

Abstract

Otoacoustic emissions (OAEs) are acoustic waves measured in the ear canal which are generated in the ear. These emissions are used in clinical hearing examinations. If they are not present, it signalizes a problem with hearing which is then analyzed deeper. However, otoacoustic emissions may not only serve as a screening tool but can also be used to objectively assess characteristics of the auditory periphery. For example, the latency of reflection-source OAEs provides an indirect tool for measuring the tuning of cochlear filters. This work introduces and verifies two methods for obtaining reliable delays of OAEs, developed by Shera and Bergevin (2012): the peak-picking algorithm and the cepstral analysis method. Shera and Bervegin (2012) verified the methods using simulated OAEs derived from a linear cochlear model. Here we use a nonlinear cochlear model, which allows us to study how the latency of the OAEs depends on the level of the evoking stimulus. For simulated emissions, the results are relatively precise when comparing them to estimated reference values. The methods were applied even on experimentally measured data that confirmed the validity of the used emission model.

Keywords: otoacoustic emissions, phase-gradient delay, phase smoothing, cochlear filters

Table of contents

Introduction

When a sound represented by an acoustic wave enters a human ear, it is first processed by the peripheral ear, transforming the wave into a neural signal. However, the peripheral ear is not only a receiver but can also emit a weak sound. This sound, called the otoacoustic emission (abbreviated as OAE), can be recorded by a microphone placed into the ear canal (Probst et al., 1991). OAEs are generated by the shivering of the eardrum, which emits vibrations returning from the cochlea through the middle ear's ossicles. OAEs are assumed to be a byproduct of cochlear amplification, a phenomenon that should play a crucial role in the hearing system's extraordinary sensitivity and frequency selectivity. It means that some vibrations traveling to the organ of Corti are not absorbed and transferred to the neural system but change the direction towards the outside of the ear (Kemp, 2002).

OAEs can be considered an objective window into the human cochlea's functionality, which leads to their utility in examining the cochlea in a non-invasive way. This fact brings us a helpful method of hearing analysis besides the other standard techniques used (Probst et al., 1991).

Apart from screening in clinical examinations, OAEs are used to obtain tuning of cochlear filters. The slope of the OAE delay is tightly bound with the cochlear filter tune-up (Shera et al., 2010). In this work, the OAE phase-gradient delay is examined. We can estimate the filters' tune-up if we measure OAEs generated by reflection because their phase rotates rapidly, and their phase-gradient delay equals twice the delay of the basilar membrane (BM) transfer function. Two methods of obtaining the phase-gradient delay of OAEs – the peak-picking algorithm and cepstral analysis smoothing – are implemented and are freely available to the public (see Conclusions). These methods were previously used to obtain phase-gradient delays for OAEs from a linear cochlear model (Shera & Bergevin, 2012). We apply the methods to simulated OAEs from a nonlinear cochlear model and study the effect of intensity change. The phase-gradient delays are also estimated for experimentally measured OAEs from human subjects.

1 Otoacoustic emissions

This section introduces otoacoustic emissions. Further information about the anatomy and physiology of hearing is described in the Appendix. Different types of OAEs are known depending on the specific properties described in this section. All of them are evoked in their particular way and behave diversely. Later there will be two types of OAE generation discussed.

1.1 Classification of OAEs

We generally recognize two types of otoacoustic emissions (Probst et al., 1991): spontaneous OAEs (SOAEs) and evoked OAEs (EOAEs). The mechanism of SOAEs' generation is not known enough yet. SOAEs will not be discussed further in this thesis because they can be missing even when people have no trouble with hearing (only around 70 % of people with no hearing problems have them), decreasing their reliability (Talmadge et al., 1993). Based on that, they are not used in medical diagnosis, so we will not focus on them. On the contrary, the evoked OAEs are produced by a provided external stimulation.

The EOAEs can be recognized according to how they are evoked, i.e., the type of stimulation that produces them. Three stimulus types are most commonly used. The first type is the distortion-product otoacoustic emissions (DPOAEs), which will not be the topic of this thesis (but will be briefly presented in Section 1.1.1). On the contrary, the two types of interest that will be examined are stimulus-frequency (SFOAEs) and transiently evoked (TEOAEs) otoacoustic emissions (Probst et al., 1991).

According to the literature, an interesting fact about the EOAEs is raised. The evoked otoacoustic emissions can be generated in two ways: by nonlinear distortion or linear reflection, dividing them into two main groups: distortion-source otoacoustic emissions and reflection-source otoacoustic emissions (Shera & Guinan, 1999). The details of the OAE taxonomy are illustrated in Figure 1.

1.1.1 Types of EOAE generation

When OAEs are produced by nonlinear distortion, we call them distortion-source emissions (Shera & Guinan, 1999). Into this category, we assign the DPOAEs. This phenomenon of nonlinear distortion is considered to be associated with the outer hair cells' transduction in the organ of Corti. Distortion-source emissions are created based on physiological nonlinearities caused by the cochlear amplifier. Assuming that the cochlea's response is nonlinear, mechanical distortions of the traveling waves arise. These mechanical distortions may result in backward-traveling waves later recognized as the emissions themselves.

On the other hand, OAEs can also be generated by linear reflection (Shera & Guinan, 1999). A significant difference compared to the nonlinear distortion is that a part of the forward-going traveling wave energy can be turned in the opposite direction because of coherent reflection from impedance perturbations along the BM. These perturbations are caused by mechanical irregularities in different parameters of the organ of Corti (e.g., amplification, stiffness). We consider SFOAEs and TEOAEs as members of this emission group.

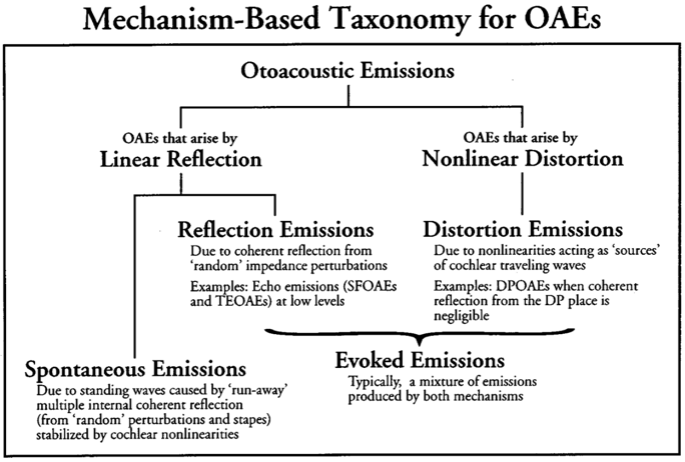

Figure 1: Hierarchy of the OAE generation taxonomy. The word "source" is omitted in both reflection and distortion emissions, but reflection- and distortion-source are meant. Taken from (Shera & Guinan, 1999).

Generally, emissions measured at lower stimulus levels contain energy from the linear reflection. The distortion emissions are primarily generated when the reflection at the frequency of the distortion can be neglected. It is also possible to have otoacoustic emissions from a mixture of both discussed generation types, such as DPOAEs (Shera & Guinan, 1999).

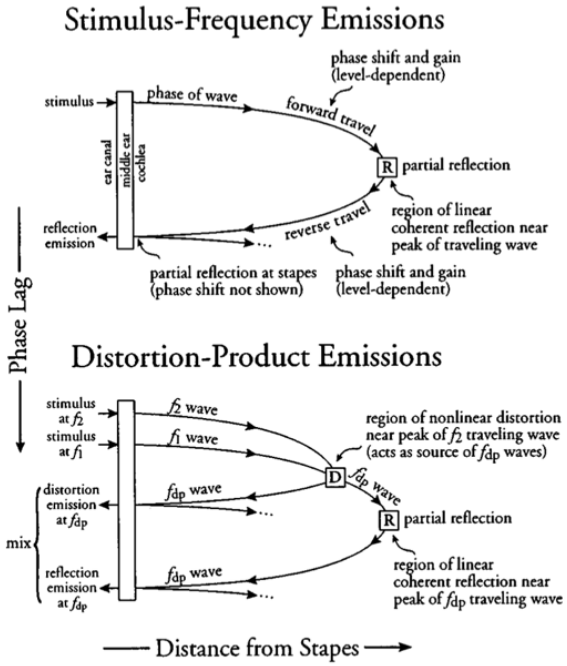

Figure 2: Generation mechanism of SFOAEs and DPOAEs. The origin of the SFOAE reverse wave is demonstrated as a partial reflection (R) nearby the peak of the wave envelope. DPOAEs are sometimes evoked by a combination of a nonlinear distortion (D) and a linear coherent reflection (R). Taken from (Shera & Guinan, 1999).

Figure 2 shows the generation of both SFOAEs and DPOAEs. Here, SFOAEs are generated by a linear coherent reflection, whereas the DPOAEs have a nonlinear distortion as their primary source and a linear coherent reflection as their secondary source. DPOAEs are evoked with two pure tones of nearby frequencies (the typically used ratio of frequencies is approximately 1.2). First, the distortion arises in the place along the BM where the traveling waves evoked with the stimulus overlap (described with the letter D). After that, a part of the traveling wave is turned in the opposite direction (backward-traveling), and a part continues in the forward direction to the place along the BM, which maximally responds to the distortion frequency. In mammals, the most salient distortion is at cubic difference tone at $f_{dp} = 2f_1 - f_2$, where f_1 and f_2 are frequencies of evoking pure tones. Part of the traveling wave can be reflected from impedance perturbations at this tonotopic place (described with the letter R). This means the distortion and reflection happen at different places along the BM.

1.1.2 SFOAEs

Stimulus-frequency otoacoustic emissions are evoked by a continuously stimulating pure tone of a low level (supplementary acoustic energy at the exact stimulus frequency point) which makes the main difference compared to other EOAEs.

Figure 3 displays the amplitude and phase of SFOAE data measured in a human subject. The amplitude is expressed as SPL (sound pressure level) in decibels, the phase in cycles. SFOAEs are assumed to be generated due to reflection from impedance irregularities randomly distributed along the BM. The backscattered wavelets from the irregularities may vary in their phase. Their relative phase then determines whether the wavelets add constructively or destructively. The SFOAE phase quickly rotates, which, together with the so-called amplitude fine structure, can be explained by the reflection mechanism (Shera & Zweig, 1993). One of the main aims of this work is to estimate the latency of the SFOAE phase reliably.

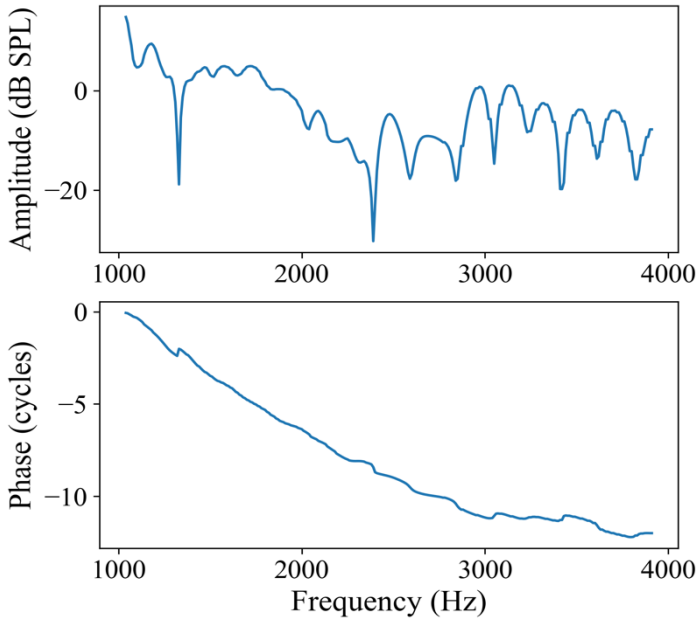

Figure 3: SPL and phase of experimental SFOAE data. The SPL was calculated from data measured in dB re 20 µPa. The phase is given in cycles traveled. The examined subject had normal hearing.

1.1.3 TEOAEs

The second category of OAEs that will be a subject of interest in this thesis is transiently evoked otoacoustic emissions. This type of otoacoustic emissions was the first to be discovered at the beginning of OAE research (Kemp, 1978). TEOAEs have been given their name mainly thanks to the character of the stimulus that produces them. This transient stimulus refers to a brief sound stimulus presented to the ear and elicits a response from the cochlea. These short sounds are usually presented as tone bursts or clicks and are designed to stimulate the cochlea over a broad range of frequencies. Out of the used stimuli, the most common are sinusoids and Gaussian- or rectangular-shaped clicks. Based on the length of the stimulating tone, the TEOAEs are distinguished into different classes having various properties (Probst et al., 1991). An essential utility of TEAOEs is the newborn screening of hearing.

This work examines clicked evoked OAEs (CEOAEs) responding to a provided click (see Figure 4 for details of CEOAE amplitude and phase). To delete the click from the response, a window is applied to take only a signal from a specific time location, where the click should not be present anymore. Need to say that CEOAEs (TEOAEs in general) and SFOAEs are very similar in amplitude and phase (Charaziak & Shera, 2021).

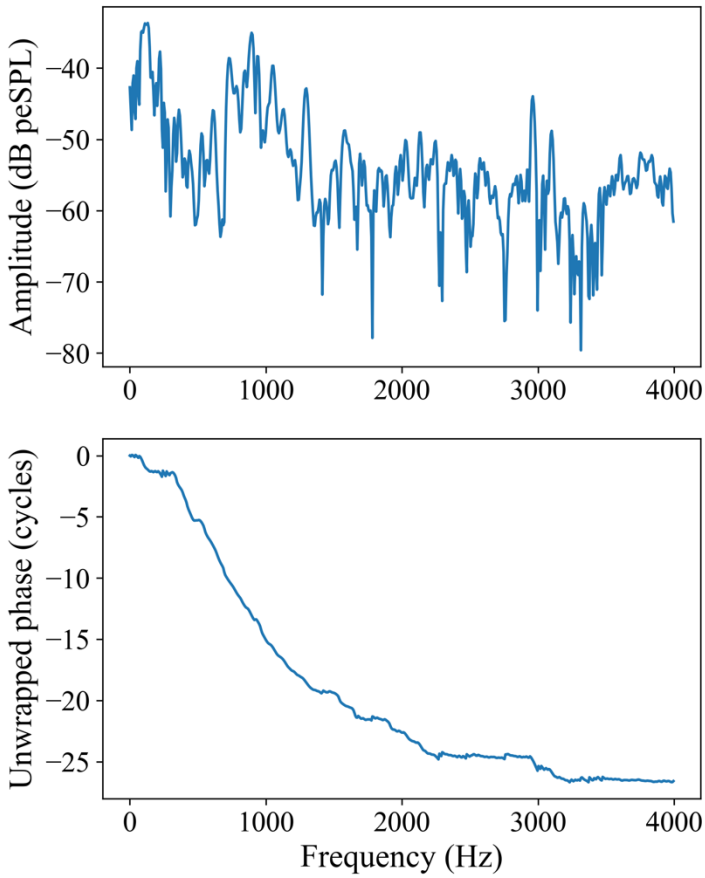

Figure 4: Peak equivalent SPL (peSPL) and unwrapped phase of experimentally measured CEOAE. Data were obtained from time-domain CEOAE data and displayed as a dependency on frequency.

2 Application of OAEs in medicine

Otoacoustic emissions are very useful in examining human hearing. They can inform us about the mechanical features of the inner ear cochlea and the functionality of its outer hair cells. Their existence is very beneficial because most of the peripheral defections of human hearing come from the cochlea's sensory part. Based on that, OAEs are applied in examination methods for clinical hearing problem-solving (Probst et al., 1991).

The main advantage of this diagnostic approach based on OAEs is that it is an objective method, which means there is no need for the patient to communicate with the examiner actively, and it is not required to consider the patient's response to a sound test. Also, it is a noninvasive technique, making the patient more comfortable with it. This fact is mainly used when screening the hearing of newborns who, indeed, are not able to talk or interact in any other sort of way. The whole examination process is that a little probe (an earphone) is placed into the patient's ear, then it plays a sound into the ear while waiting for the response to return (see Figure 5). With a receiving device, it measures the OAE signal, which is the fundamental interest of the whole examination. For screening purposes, only the presence of the emissions is examined. There probably should not be any problem in the peripheral ear if OAEs are present and our hearing is normal. The American Speech-Language-Hearing Association claims that otoacoustic emissions should not occur if hearing loss is more significant than approximately 25-30 decibels. Suppose the test results appear unfavorable, i.e., OAEs are hardly measured or missing. In that case, a problem with the hearing system is probable. Other examination methods are usually applied to verify this result and resolve the source of the problem if it exists (ASHA, 2023).

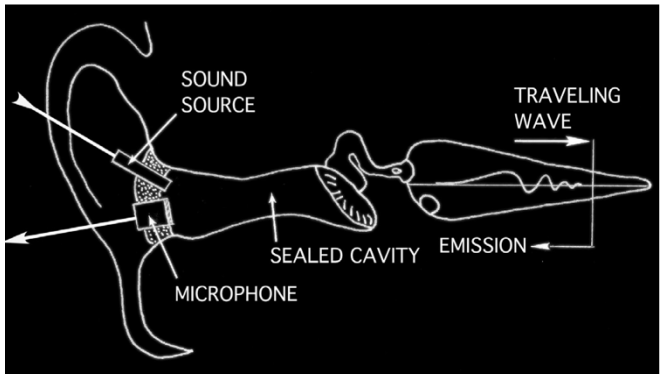

Figure 5: Scheme of the OAE measurement. The probe is placed into the ear canal, and a sound is played from a specific source. After the OAEs are generated, they are captured by the probe's second part – a microphone. The picture was taken from the web of Acoustics Today (available at: https://acousticstoday.org/wp-content/uploads/2017/08/Martin.pdf)

3 Methods for obtaining phase-gradient delay

In this thesis, we are interested in the otoacoustic emissions evoked by reflections. An exciting feature of OAEs evoked by linear reflection is their phase-gradient delay. It indicates the physical traveling time of the evoking stimulus into the place where the emission is generated, plus the traveling time of the emission out of the cochlea. This section presents two methods Shera and Bergevin (2012) introduced as a reliable estimation of OAE phase-gradient delay. All method steps, calculations, and graphical results were obtained with the help of Python programming language.

3.1 Importance of phase-gradient delay

The mechanisms of linear reflection (with a preexisting perturbation) and nonlinear distortion (wave-induced source) are compared in Figure 6. In the case of preexisting perturbations, when we change the wave's frequency, the phase changes as well. The perturbation stays at the same BM location, and the wave is reflected with a different phase. On the contrary, for the wave-induced source, the source is carried with the wave. Here, with a frequency change, the phase stays the same (Shera & Guinan, 2008).

The fact that the perturbation stays fixed in a specific cochlear location means that the phase-gradient delay of reflection-source OAEs is two times greater than the phase-gradient delay of BM (cochlear filters) transfer function (Shera & Guinan, 2003). Thanks to that, we can objectively estimate the tune-up of cochlear filters (sharpness of cochlear frequency tuning), as is indicated in Figure 7. As is demonstrated on harmonic oscillators with different resonant frequencies, the steeper the phase's slope is, the narrower the magnitude of the transfer function is. In other words, sharper cochlear filter tuning corresponds to longer OAE delays (Shera et al., 2010).

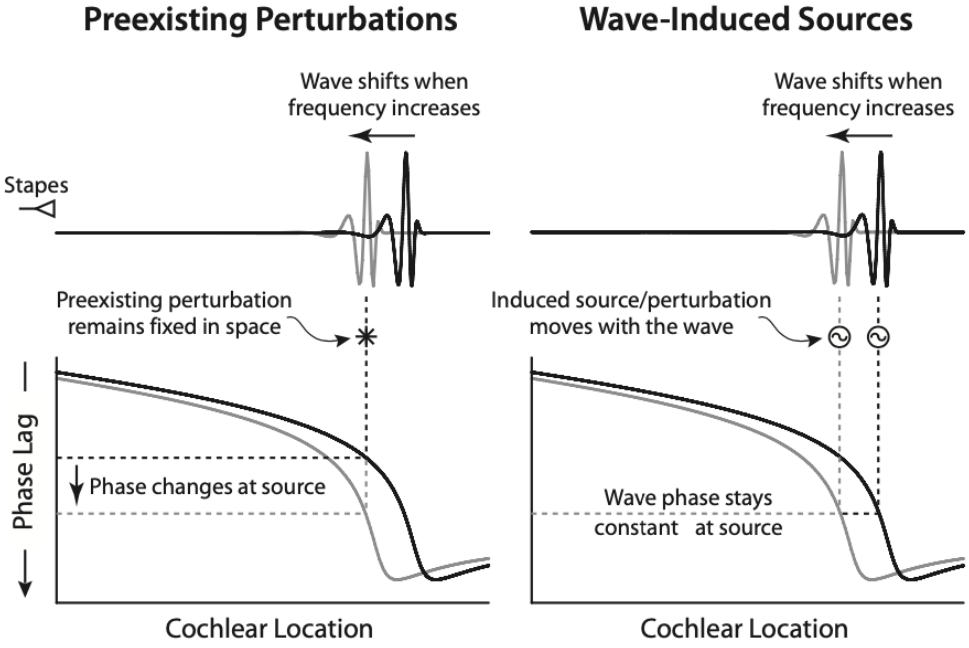

Figure 6: Comparison of two OAE generation types: linear reflection (left) and nonlinear distortion (right). Taken from (Shera & Guinan, 2008).

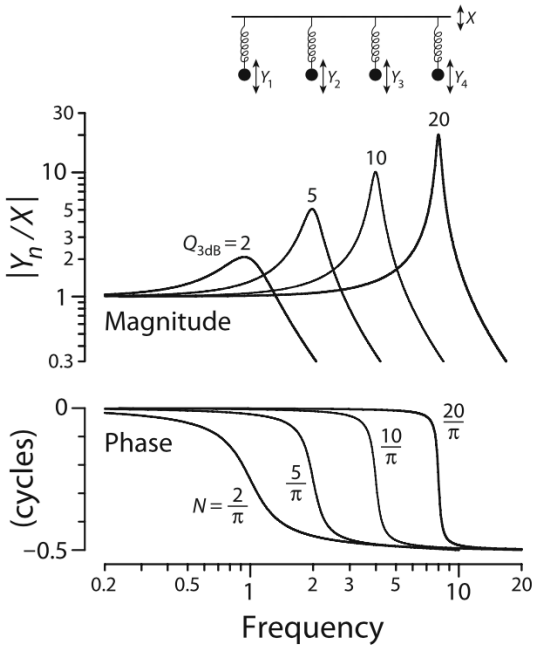

Figure 7: Dependency between OAE phase-gradient delay and cochlear filter tune-up (marked with letter Q). Taken from (Shera et al., 2010).

Interestingly, phase-gradient delays of OAEs due to reflection are significantly longer in humans than in other mammals. As mentioned, this is equivalent to sharper tuning, which allows us to understand our speech correctly (Shera & Charaziak, 2019).

3.2 Obtaining phase-gradient delay

This thesis presents SFOAEs and CEOAEs derived from a mathematical cochlear model and measured in human subjects. The used mathematical cochlear model is nonlinear, and an analytical solution for SFOAEs is known for this model (see Section 4.1 and Vencovský et al., 2023). Therefore, we can distinguish different mechanisms of emissions generation and study their interaction when the stimulus intensity is changed. The analytical solution allows us to point out the influence of multiple reflections and verify technics for its discard (the cepstral analysis method used in this work).

As Figures 3 and 4 show, OAEs can be represented in the frequency domain as a function of the frequency of the evoking stimulus. For SFOAEs, the frequency domain representation can be obtained easily by expressing their amplitude and phase at a given stimulus frequency. For CEOAEs, we obtain a time-domain response during the measurement, which can then be transformed into the frequency domain by Fourier transform (FT). The phase-gradient delay is calculated from the unwrapped phase by this equation:

$$\tau = -\frac{1}{2\pi}\frac{\partial \angle S}{\partial f}, \tag{1}$$

where τ is the phase-gradient delay, $\angle S$ is the unwrapped phase of the frequency spectrum, and f is frequency.

To calculate the delay, following Equation 1, we have to compute the phase derivative with respect to frequency. Because we are working only with discrete measurements, we cannot simply apply the continuous derivation, but we have chosen to use the first-order central difference gradient. The final look of the phase-gradient delay computed for the simulated SFOAE data is illustrated in Figure 8.

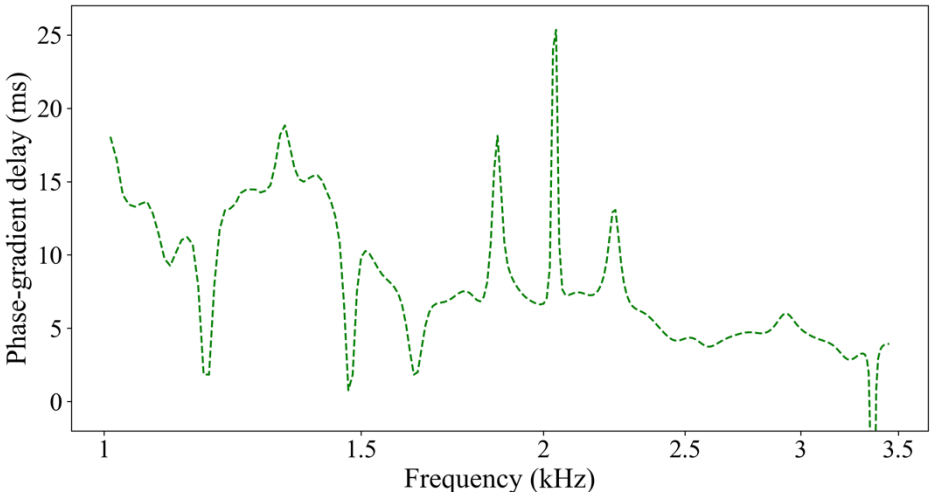

Figure 8: Overview of the phase-gradient delay. Here, results for the 20 dB SPL of simulated SFOAEs are displayed.

As was mentioned at the beginning of this section, the phase-gradient delay of the reflection source OAE phase reflects the phase delay of BM transfer functions (cochlear filters) at that frequency. Here we show how we estimated the phase-gradient delay of BM transfer functions, which are then used in this thesis as a "reference" for comparison with the phase-gradient delay of the OAE phase. To explain its background more deeply, the BM transfer function is a fraction of the BM and stapes displacements. To determine its delay, we have to search for the global maximum of the absolute value of the transfer function and evaluate the phase-gradient delay in this point of interest. After that, we reach the reference value, whose double value will be compared with the methods solutions. This reference solution was extracted from data with isolated frequency values in the given frequency range. In Figure 9, the process of the global-maximum search is shown with the BM transfer function for 20 dB SPL at 2 kHz.

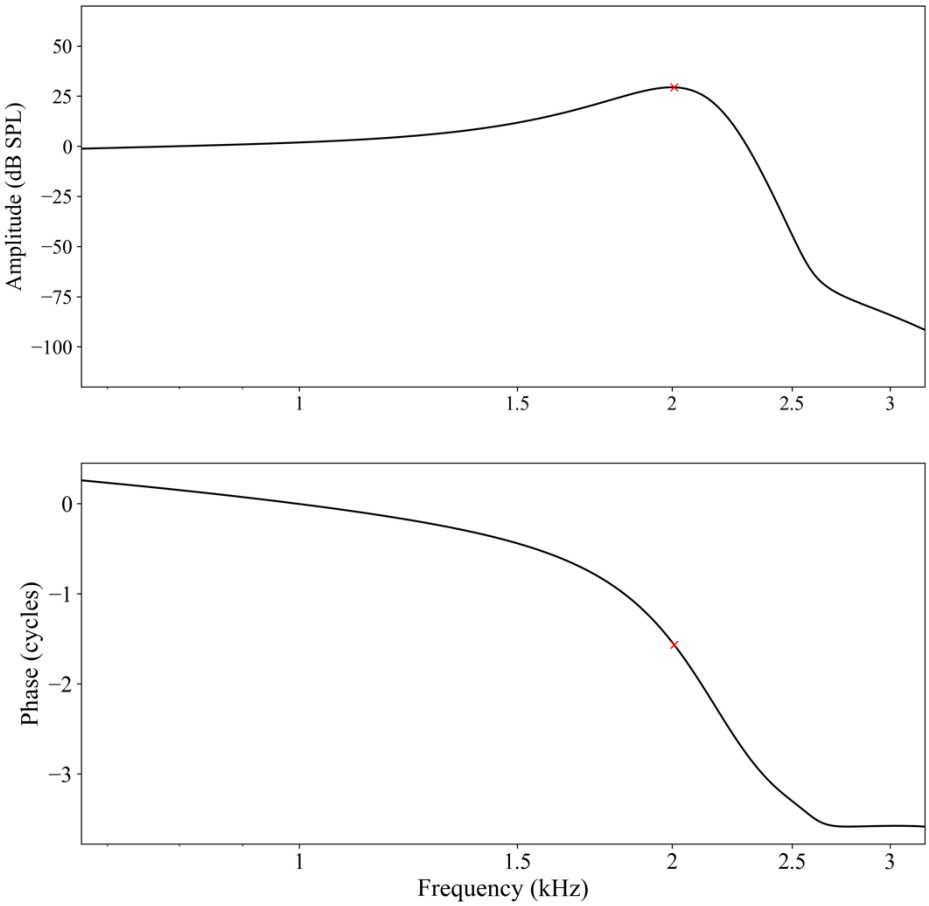

Figure 9: Amplitude and phase characteristic of cochlear filter transfer function (or BM transfer function). The filter was tuned to 2 kHz. The only peak of the BM transfer function was found to determine the frequency location of the reference delay value.

Figure 10 displays the extracted reference values for 20 dB SPL. Here, the reference is given directly in the double value of the BM transfer function delay result, which is then compared with the results of the methods used. As can be seen, the assumed delays were computed for only fixed frequencies.

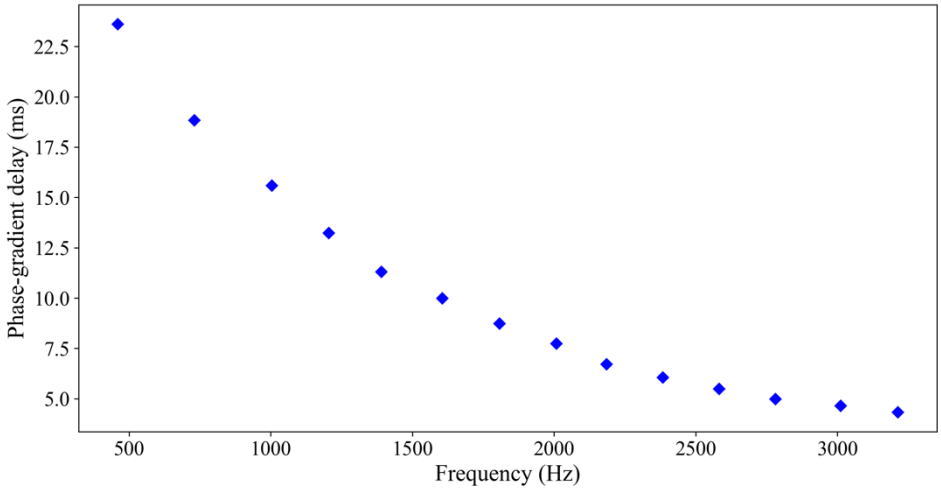

Figure 10: Assumed reference values of the phase-gradient delays. These values are compared with the results of methods used.

Two methods were applied to estimate phase-gradient delays: the peak-picking algorithm and cepstral analysis smoothing. The first one is set as the main because we use its part in the other mentioned. We can call it a raw peak-picking method since it is used alone with no additional pre-preparation of given OAE data. On the contrary, in the smoothing method, we apply a given procedure to modify the input signal to a more convenient form. Then, we examine the region of interest pointed out by the peak-picking algorithm (taken from and compared with the original OAE data).

3.3 Peak-picking algorithm

The first method used to obtain phase-gradient delays of the OAE data is called the algorithm of peak-picking, which examines the delay values in the neighborhood of local maxima of the fine structure of OAE amplitude (see the upper panel in Figure 11). It is inspired by an observation that delays at OAE SPL local maxima frequencies are supposed to be the closest to the expected reference. In peak locations, most wavelets come from the maximum of the traveling wave (TW). Here we want to estimate the phase of cochlear filters. If there are a lot of irregularities close to each other, then the reflected wavelets do not cancel each other out of phase. The wavelets also have a high amplitude, which should lead to strong emissions. On the contrary, in the neighborhood of minima, the wavelets reflected in different locations of the TW are being summed up, and they have mostly a lower amplitude, or they are canceled out. These cancellations cause sudden jumps in phase, as illustrated in Figure 11 (Shera & Bergevin, 2012).

The initiating step of the algorithm is to find the local maxima of the OAEs and pick several samples surrounding them. For instance, we have decided to investigate the area of three points around the maxima, including the maximum itself. Figure 11 shows that the peaks were correctly found with their neighbors (because of the model, artificial units are used – described more in Section 4.1). The phase-gradient delays are calculated at the picked frequencies.

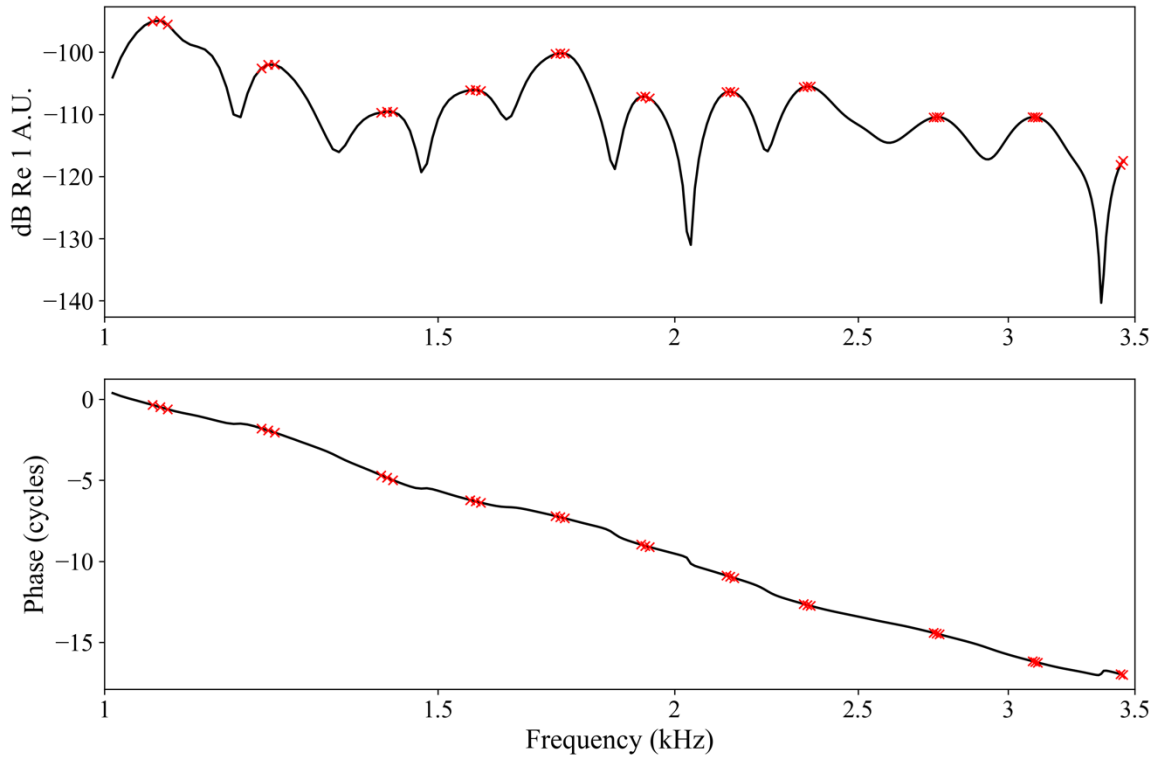

Figure 11: Peak-picking applied to the simulated SFOAE data of 20 dB SPL. Only the local maxima‘s direct neighbors (three points in total) were chosen (top). The unwrapped phase in cycles is shown (bottom) in the found points of interest (red crosses).

3.4 Smoothing with cepstral analysis

The motivation for this method is that during the generation of OAEs in the cochlea, a standing wave can occur by a wave reflection between the interface stapes-cochlea and the location where the OAEs are generated. In that case, the peak-picking algorithm estimates the latencies wrongly. Shera and Bergevin (2012) proved that cepstral analysis provides a way to suppress the influence of these standing waves.

3.4.1 The mathematical aspect of cepstrum

This method is based on the well-known cepstral analysis, whose primary goal is separating signals containing echoes. The main idea is to process the logarithm of the frequency response using the logarithm's feature allowing us to break down a product into a sum. We are applying this method because additional reflections in OAEs cause a rippling pattern in OAE amplitude, and cepstral analysis should identify these components. These ripples depend on the phase trend. In general, cepstral analysis finds periodicities in the spectrum and reveals the ripples allowing us to discard them.

Usually, we apply FT on a time domain signal. We must introduce another domain during cepstral analysis because we apply the FT on the signal in the frequency domain (OAEs in our case). We call it quefrency η, which we get after computing the FT of a frequency spectrum.

3.4.2 Method details

This section describes the cepstral analysis method that Shera and Bergevin (2012) presented. This method provides a computationally non-expensive way to address the problem with multiple reflections. Figures 3 and 4 show that the OAE phase versus frequency function is curved. Because of that, we first transformed the phase into a new variable φ, the original smoothed and unwrapped phase. Here we have chosen the Savitzky-Golay filter in accordance with Shera and Bergevin (2012). We used the window of length 5, which means that the filter is fitting a polynomial to 5 adjacent data points at a time. The polynomial order was set to 1 because the unwrapped phase should more or less resemble a linear function. We transferred φ into cycles thanks to division by 2π and switched the sign making it an increasing sequence. The monotonicity of the transformed φ was supposed to be assured by the smoothing. Still (as shown in Figure 12), we had to erase some of the data making φ an increasing sequence. Then, to have φ evenly spaced, we resampled it, taking values up to the first local maximum (located after the chosen target frequency). Unfortunately, we have lost some of the data, leading to fewer peaks found by the peak-picking method.

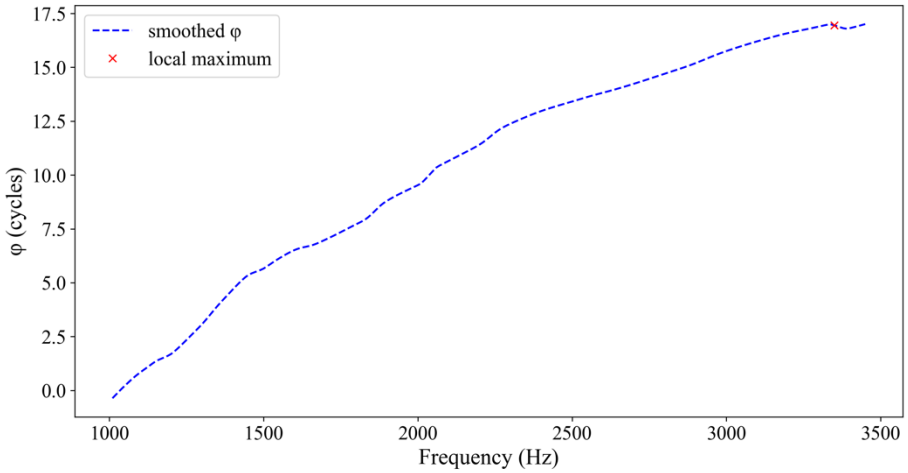

Figure 12: Smoothed and transformed phase to a new φ variable. Because an increasing sequence was required, local maxima had to be erased from the data.

As mentioned before, in this method, we were interested in examining the logarithm of the OAE. Recall that we are computing a logarithm of complex numbers, which can be divided into a sum of the logarithm of the absolute value and the imaginary unit multiplied by their phase. This equation describes the process:

$$logS^0_{OAE} \cong F^{-1}\{WF\{logS_{OAE} + 2\pi i\varphi\}\} - 2\pi i\varphi, \quad (2)$$

where F [F^{-1}] represents the [inverse] fast Fourier transform (FFT), and W is the cutoff window applied in the quefrency domain.

So, first of all, we have calculated the spectrum's logarithm. Because the FFT was computed concerning the φ variable, we had to assure ourselves that the OAE logarithm depended on it. To do that, we interpolated it along the φ axis using cubic spline interpolation. Separating the interpolation for the real and imaginary parts was necessary because the imaginary one had to be unwrapped to correspond with the unwrapped φ variable.

The literature states that applying FFT separately for real and imaginary components is convenient (Shera & Bergevin, 2012). We followed this approach by summing both FFT results (before that, the φ variable in radians multiplied by 2π was added to the imaginary part of the spectrum). Applying FFT on the frequency spectrum brought us to the quefrency domain, the conjugate to φ variable (also called the "time" variable). Knowing the sampling rate of the previously resampled φ, we could reconstruct it and apply the primary part of this method – the quefrency filtering. We constructed a window with a cutoff at a specific quefrency location (Shera & Zweig, 1993). This window is a type of recursive-exponential filter defined by this equation:

$$W_n(\eta;\eta_c) \equiv 1/\Gamma_n(\lambda_n\eta/\eta_c), \quad (3)$$

where n is the filter order, η_c is the window cutoff, λ_n is the scale factor, and Γ_n is obtained from the following recursive function:

$$\Gamma_{n+1} = e^{\Gamma_n - 1}, \quad \text{with} \quad \Gamma_1(\eta) = e^{\eta^2}. \quad (4)$$

The quefrency cutoff was estimated by the number of cycles traveled by the φ variable multiplied with a cutoff coefficient set to 0.9 to compare. Figure 13 shows the calculated recursive-exponential window, which would suppress quefrencies above the cutoff.

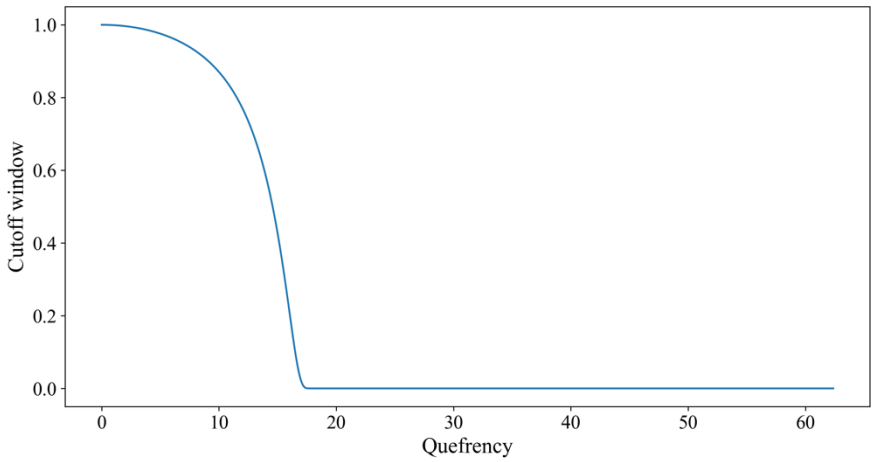

Figure 13: Cutoff window in the quefrency for simulated SFOAEs. Here, the cutoff coefficient was set to 0.9 times the number of cycles the new φ variable traveled.

The final step of the cepstral analysis method was to return to the OAE logarithm. The inverse FFT concerning φ was computed for the quefrency data taking us back to the frequency domain. According to Equation 2, wrapped φ had to be subtracted (compensating the initial addition to the logarithm before FFT was used). Recall that it is wrapped because the original spectrum consists of the wrapped imaginary component. In Figure 14, the comparison between the original and smoothed logarithms (for simulated SFOAEs) is displayed with a dependency on φ in cycles.

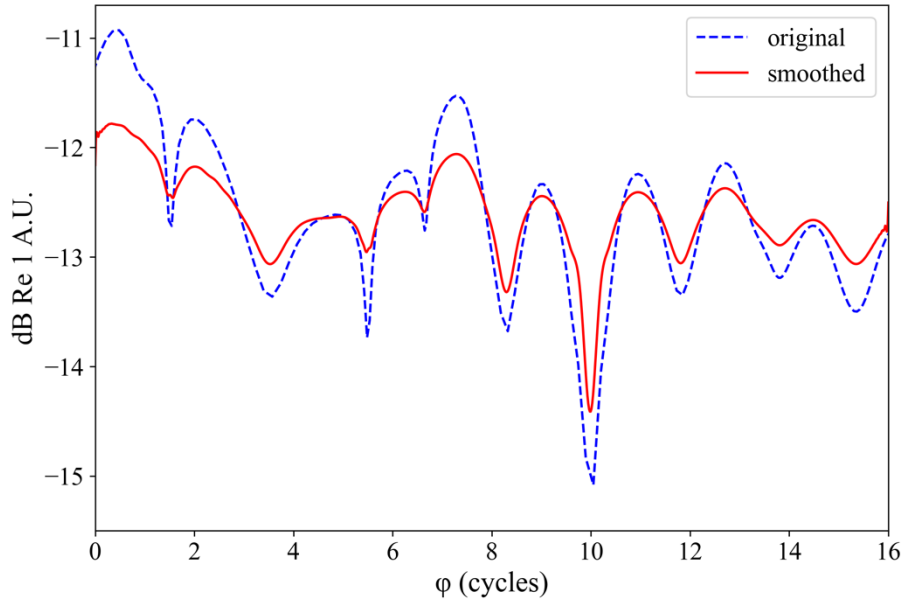

Figure 14: Comparison of original and smoothed simulated SFOAE logarithm.

Because we are interested in comparing phase-gradient delays of the OAE data, not its logarithm, we transformed the smoothed result by applying an exponential on it. We can see in Figure 15 that the cepstral analysis shortened phase-gradient delays at lower frequencies (below 1.5 kHz) in comparison with the original latency values.

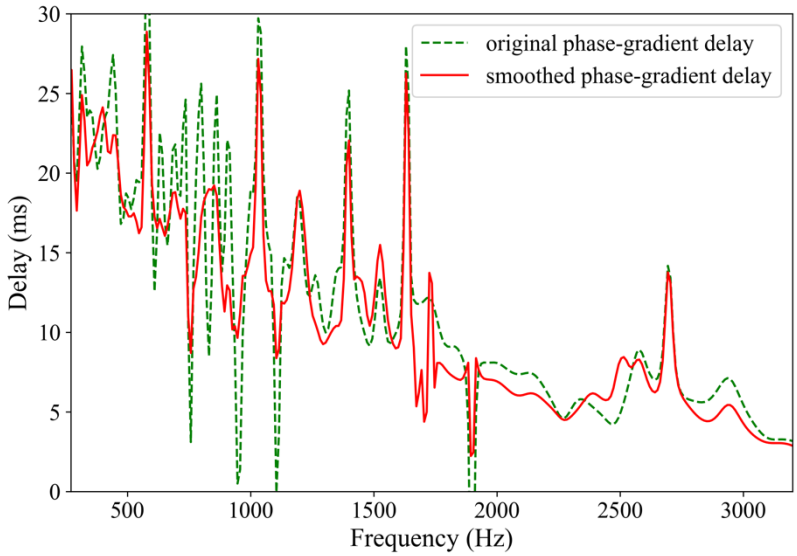

Figure 15: Comparison of the original and smoothed logarithm of simulated CEOAE data.

4 Results of used methods

4.1 Model

This section verifies the chosen methods for latency estimation by using SFOAEs and CEOAEs derived from a nonlinear cochlear model. Shera and Bergevin (2012) used a similar approach. However, they used a linear cochlear model. Therefore, we can also study how the OAE latency changes with signal intensity (we analyzed SFOAE data from four intensity levels: 20, 30, 40, and 50 decibels). In addition, the analytical solution of the model equations for SFOAEs allowed us to separate the effect of standing waves (additional reflections) and nonlinearity on SFOAE latency (Vetešník et al., 2022).

The model solution indicates that although the linear reflection is the main source of SFOAEs, the reflected wavelets perturb nonlinear force, generating additional components due to nonlinearity. Due to nonlinearity (NL component), this component has interestingly approximately opposite phase to the component due to reflection (CR component). The overall SFOAE signal represents a superposition of these two components (Vencovský et al., 2023). Details of SFOAE, NL, and CR amplitudes are displayed in Figure 16.

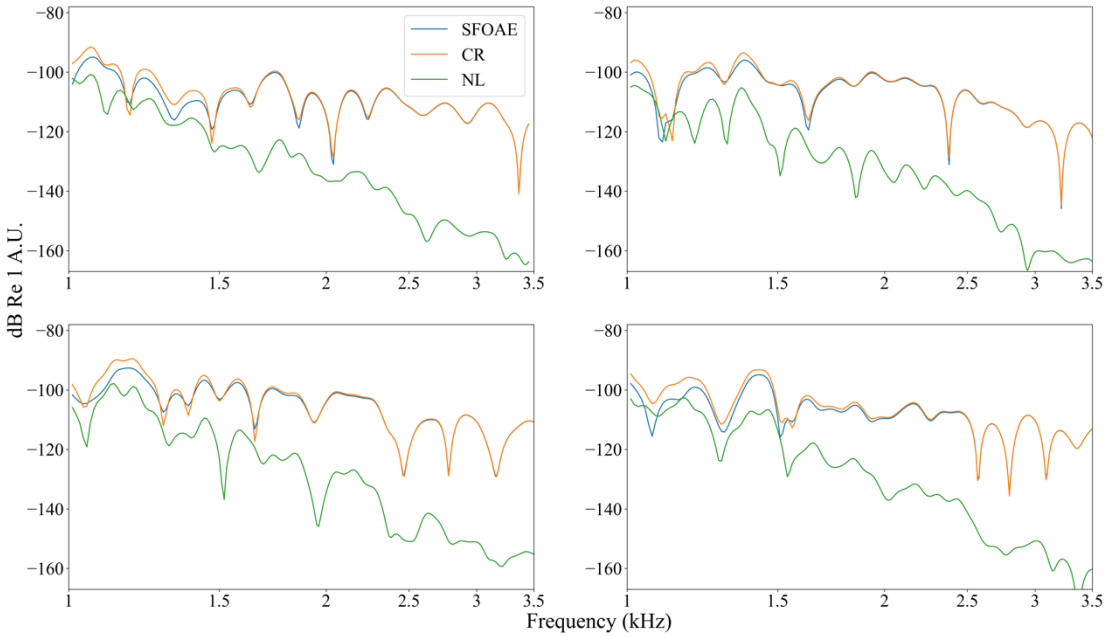

Figure 16: Amplitude of SFOAE (blue), CR (orange), and NL (green) components for simulated 20 dB SPL level. Each graph is displayed for a different inhomogeneity distribution.

A hydrodynamical cochlear model, which is used in this thesis, is described in Vetešník et al. (2022). The model is nonlinear because the undamping feedback force simulating cochlear amplification is transformed by a sigmoidal function which limits its effect at high intensities. Vencovský et al. (2023) present a solution of the model equation for SFOAEs, which separates the effect of standing waves of SFOAEs and the effect of nonlinearity. To generated SFOAEs, Vencovský et al. added impedance irregularities into the model in the form of roughness, which is randomly distributed along the model segments. The roughness is added to the undamping force. The model is not calibrated to predict always quantitively therefore, instead of Pascals, we use artificial units abbreviated as A.U. Details on the form of roughness can be found in Vencovský et al. (2023), and the remaining details on the model can be found in Vetešník et al. (2022).

4.1.1 Peak-picking results

As mentioned, apart from the SFOAE, the two components caused by reflection (CR) and caused by perturbations of the nonlinear force (NL) were also analyzed. First, it is appropriate to discuss the characteristics of the components, especially their amplitude. Figure 17 shows that the NL component has a relatively low amplitude at high frequencies for lower intensity. Because of this, the nonlinear force does not influence the result much. Compared with that, the CR component is similar to the SFOAE at higher frequencies and lower intensities, resulting in nearly no difference (Vencovský et al., 2023).

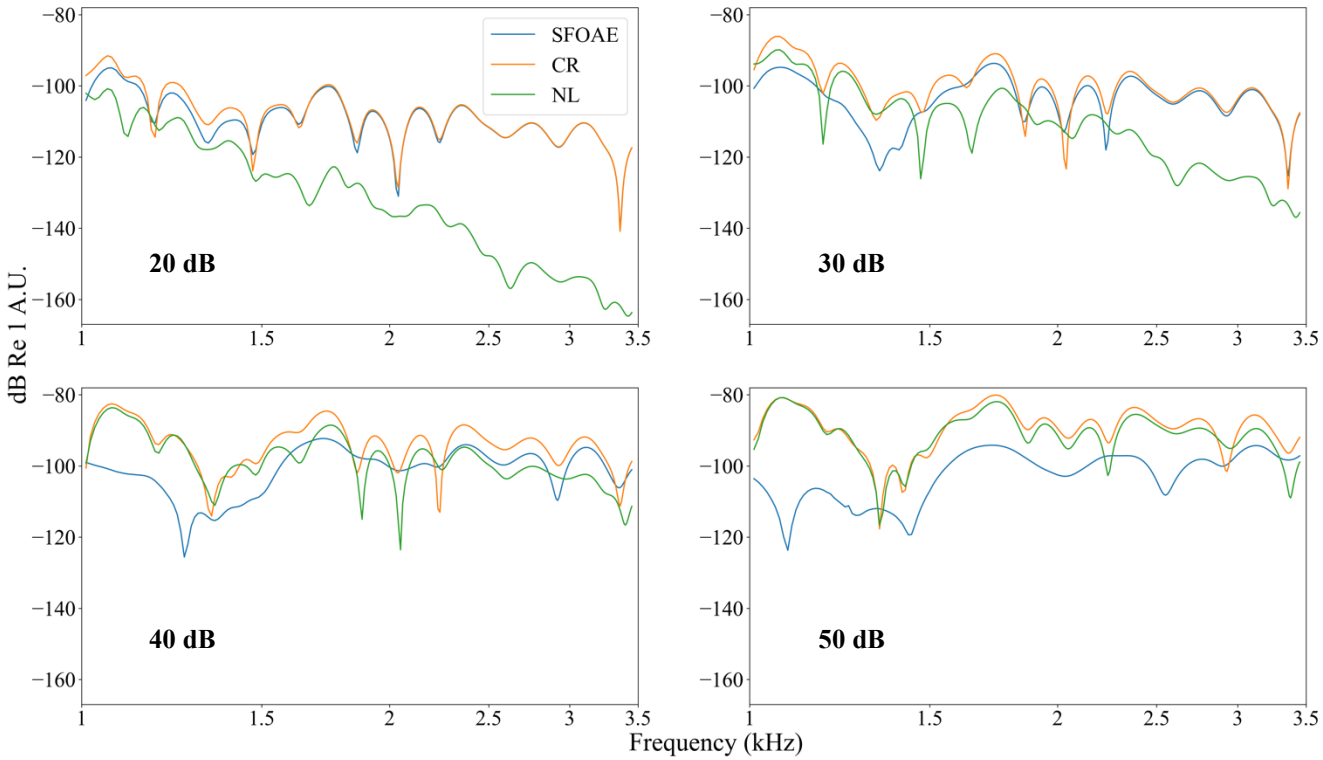

Figure 17: Amplitude of SFOAE (blue), CR (orange) and NL (green) components for all intensity levels (top left: 20 dB, top right: 30 dB, bottom left: 40 dB, bottom right: 50 dB).

Figure 18 illustrates the results of the peak-picking algorithm for simulated SFOAEs and their components (CR and NL) derived from the analytical solution of the model equations. The results are compared with the phase-gradient delay of BM transfer functions obtained at the same intensities as SFOAEs: 20, 30, 40, and 50 dB SPL.

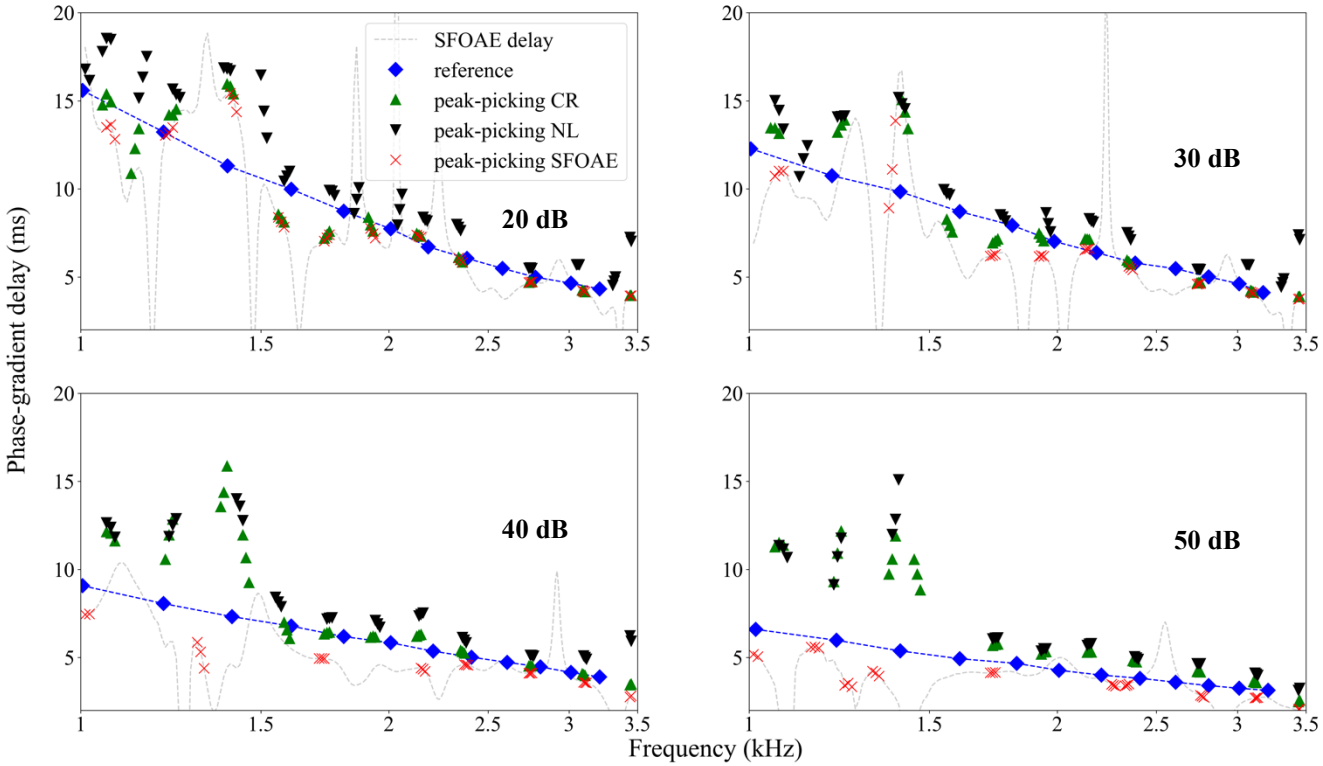

Figure 18: Comparison of phase-gradient delays for various stimulus intensities (top left: 20 dB, top right: 30 dB, bottom left: 40 dB, bottom right: 50 dB). SFOAE (red crosses), CR (green triangles), and NL (black triangles) components are compared with the reference with two times latencies estimated from the BM transfer function (blue diamonds). The gray dashed line illustrates the whole phase-gradient of SFOAE data.

Latencies of the NL component are generally longer than latencies of the CR component. It seems that as the intensity increases, the difference between the latencies of the CR and NL components gets smaller. Because the NL component is in antiphase with the CR component, the total SFOAE has shorter latencies, especially at the highest intensities for which both components (CR and NL) have similar amplitudes (see Figure 17). Note that the NL component has a comparable amplitude to the CR component at the lowest frequencies at 20 dB SPL due to higher gain at frequencies near 1 kHz than at higher frequencies (>1.5 kHz). For details see Vencovský et al. (2023). The agreement between the CR component and latency estimated from the BM transfer function proves the assumption that OAEs due to reflection can be used to predict the tuning of cochlear filters. However, due to destructive interference between the CR and NL components, the resulting SFOAEs may have shorter latency.

A more closely resembling CR component results and the reference values were expected. Looking into the results in more detail, we notice that at the lowest frequencies, the CR latencies sometimes significantly depart from the latencies estimated from the BM transfer function. Multiple emission reflections in the cochlea could explain this behavior at lower frequencies. Shera & Bergevin (2012) successfully suppressed this phenomenon using the cepstral analysis method described in the text.

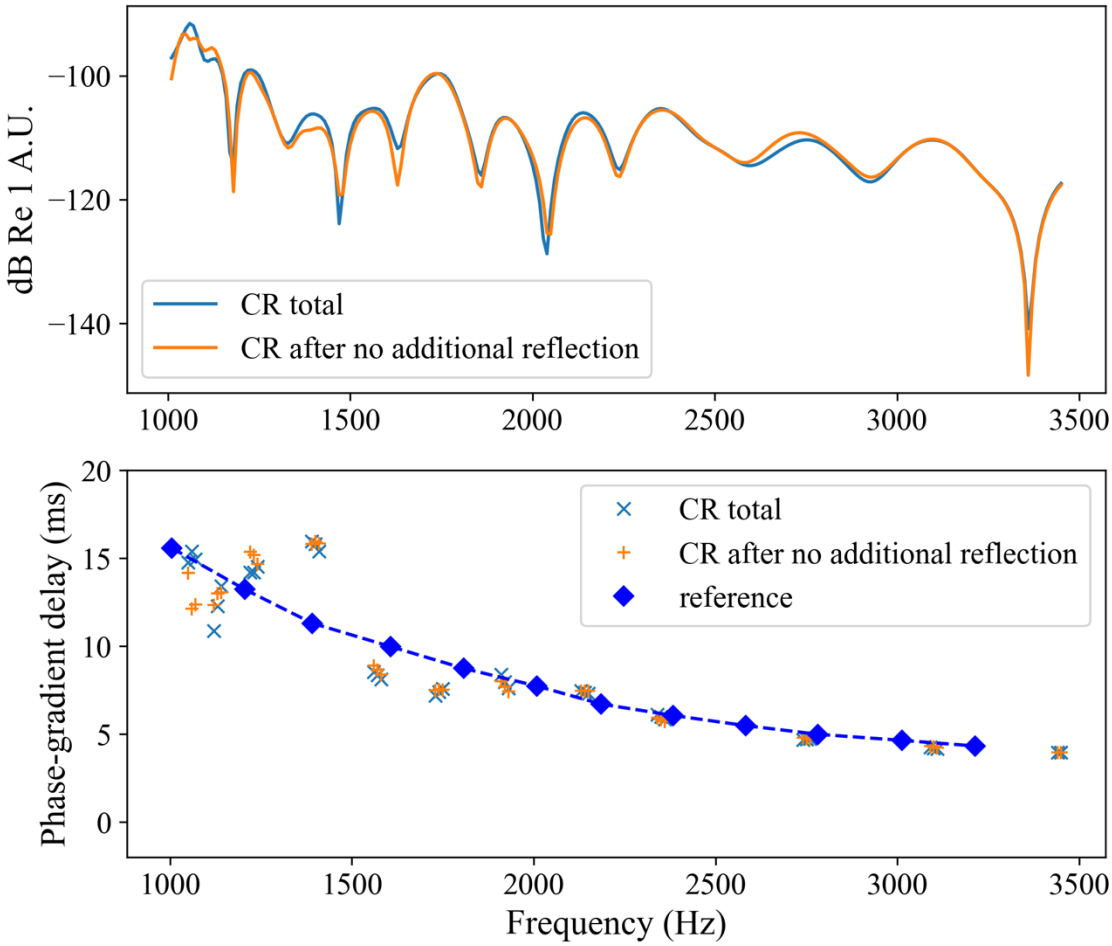

Figure 19: CR component of 20 dB level simulated SFOAE data. The total CR component (light blue) is compared with the CR subcomponent after no additional reflection (orange). The total CR component is the sum of all its subcomponents, including the one in this figure. Amplitude and the phase-gradient delay (evaluated in the location of the peaks) are compared with the reference values (blue diamonds).

We can divide the total CR component into a sum of several CR subcomponents (for the shown SFOAEs, ten subcomponents were adequate to achieve very good agreement with numerically derived SFOAEs, see Vencovský et al., 2023) that describe the situation after each additional reflection. In Figure 19, the phase-gradient delays of the total CR component at the peak locations are very similar to those of the CR subcomponent after no additional reflection (after the first wave reflection). This fact highly correlates with the components' amplitudes since they are nearly the same along the whole frequency axis. This similarity shows that multiple reflections do not cause deviation from the reference (at frequencies lower than approx. 1.5 kHz). Probably, some variability or, in other words, some measurement inaccuracy in determining the phase-gradient delay from SFOAE data is present. Because the multiple reflections do not play a big role in the emissions, the cepstral analysis method should not provide a better agreement between the simulated SFOAE phase-gradient delays and phase-gradient delays of the BM transfer function.

Because of the probable inaccuracy in estimating the phase-gradient delay from our simulated SFOAEs, it is interesting to look at different inhomogeneity distributions of the model used. Figure 20 shows the results of the peak-picking algorithm for four distributions of our simulated 20 dB SPL data. The latencies of the CR component and total SFOAE are pretty much the same at higher frequencies (1.5 kHz and more). We can see that the natural deviation from the reference delay of the BM transfer function is present in all distributions.

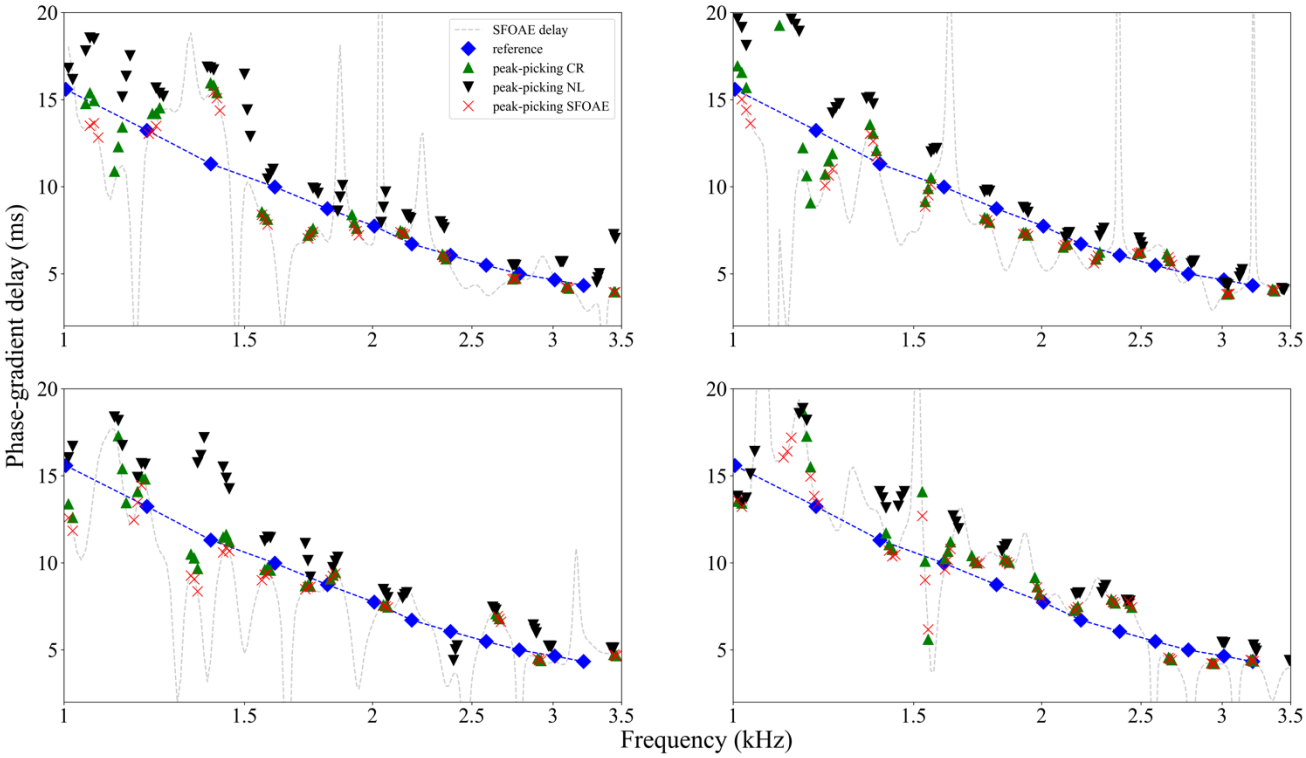

Figure 20: Comparison of phase-gradient delays of simulated SFOAEs for four different inhomogeneity distributions. Here, the 20 dB SPL data are displayed. SFOAE (red crosses), CR (green triangles), and NL (black triangles) components are compared with the reference solution (blue diamonds). The gray dashed line illustrates the whole phase-gradient of SFOAE data.

The results of the peak-picking applied on simulated CEOAEs are very precise (see Figure 21). The delays evaluated in the peak locations copy the course of the expected values. This fact even underlines the accuracy of this method applied to our simulated CEOAE data. However, when talking about delays at frequencies below approx. 1.5 kHz, they could be shortened by the cepstral analysis smoothing, which is shown in the next section.

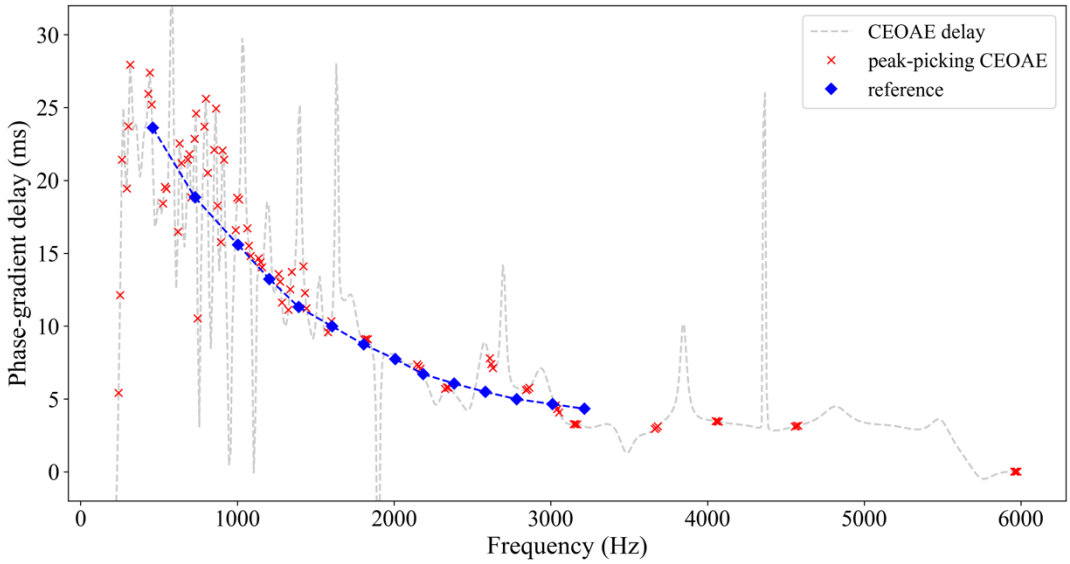

Figure 21: Comparison of phase-gradient delays for simulated CEOAE (red crosses) and the reference solution (blue diamonds). The gray dashed line illustrates the whole phase-gradient of CEOAE data.

4.1.2 Cepstral analysis results

To prove that our SFOAE simulated data is not appropriate for the cepstral smoothing method, we applied this method on 20 dB level data. Figure 22 shows no dramatic delay change at lower frequencies (below 2 kHz) when the cutoff coefficient of the quefrency cutoff window was set to 0.9. We expected that method's smoothing should help with delays at these frequencies (the latencies are usually longer here). Figure 22 illustrates that the longer delays of SFOAEs than those from the BM transfer function at about 1350 Hz were not significantly shortened after cepstral smoothing. This result corroborates our analysis of the CR subcomponent without the additional reflection presented above. We can conclude that the longer latency is not due to additional reflections. In contrast, the cepstral smoothing slightly shortened the phase-gradient delays at other frequencies.

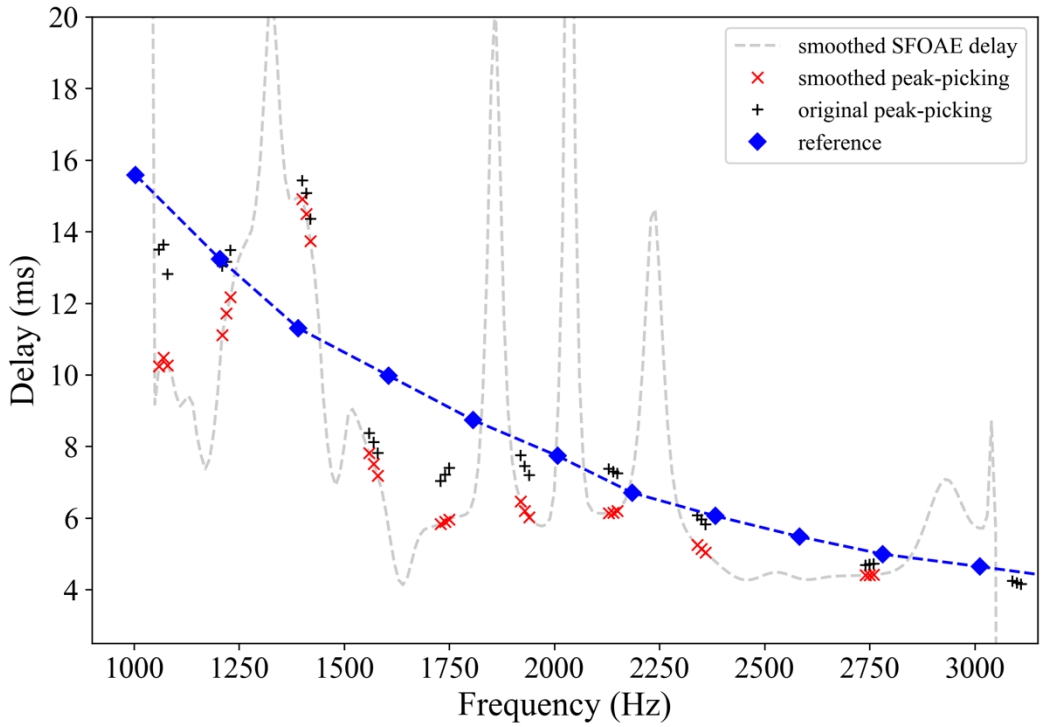

Figure 22: Results of the cepstral analysis method applied to simulated SFOAE of 20 dB SPL level. Peak values before (black plus signs) and after smoothing (red crosses) are displayed. The gray dashed line shows the total phase-gradient delay after smoothing.

On the contrary, for the used CEOAE model, the data were suitable to solve the problem with multiple reflections. Figure 23 displays the results of the cepstral analysis method applied where the cutoff coefficient of the quefrency cutoff window was set to 0.5. The comparison of the phase-gradient delays before and after smoothing is shown in the chosen frequency range (the method is focused on lower frequencies). It is observable that the delays were successfully shortened, as was expected.

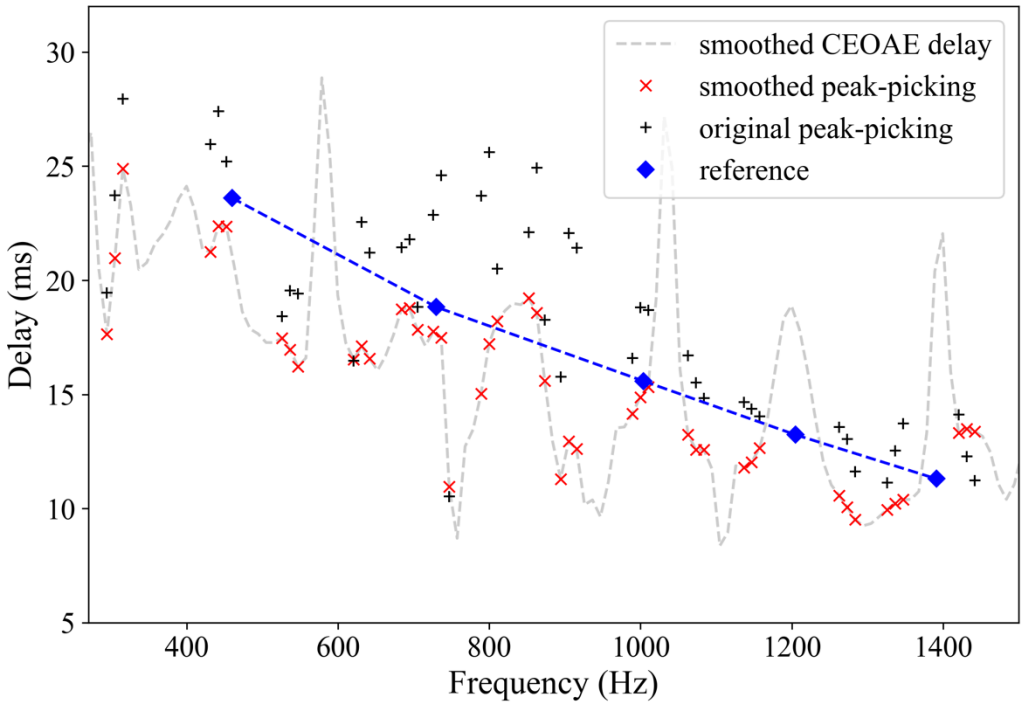

Figure 23: Results of the cepstral analysis method applied to simulated CEOAE data. Peak values before (black plus signs) and after smoothing (red crosses) are displayed together with the reference delays of the BM transfer function (blue diamonds). The gray dashed line shows the total phase-gradient delay after smoothing.

4.2 Experimental data

Three human subjects (A, B, and C) were examined – two SFOAE and one CEOAE data were analyzed. The experimental data come from normally-hearing adult subjects. The SFOAE data were measured with a suppressor tone of 60 dB SPL at 50 Hz for the probe tone. The suppression method was used to obtain the emission because it is hard to separate it from the measured signal (the signal is at the same frequency as the emission). Here, another tone with a higher amplitude is played to suppress the emission generation. As mentioned in this section, the peak-picking provided results relatively close to the expected delay values. When the cepstral analysis method was applied, nothing dramatic happened to the phase-gradient delays, which even verified that if no multiple reflections are present, the latencies are not biased.

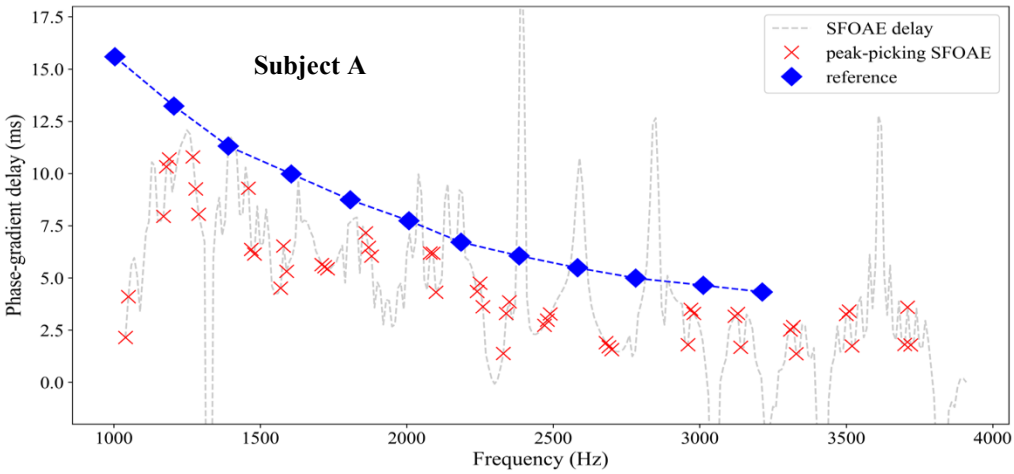

Figure 24: Comparison of phase-gradient delays of SFOAEs obtained from the peak-picking algorithm for the experimentally measured data A (red crosses) and the reference (blue diamonds). The gray dashed line illustrates the whole phase-gradient of experimental data.

In both SFOAE measurements (Figures 24 and 25), the latencies at peak locations picked out by the algorithm follow the assumed reference values. These results show that our model is pretty correct. For subject A, all latencies are shorter than the reference. On the other hand, delays of subject B surround the reference from both sides (shorter and longer).

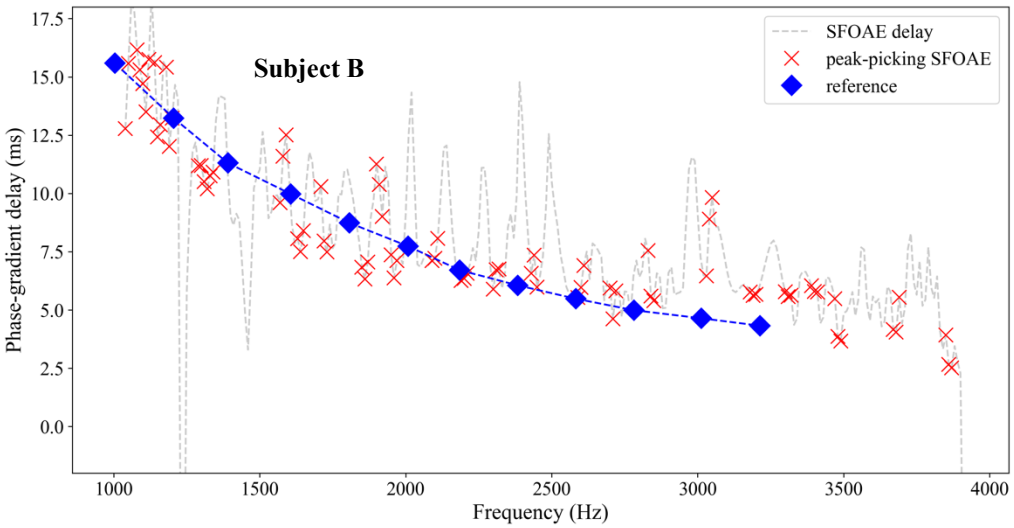

Figure 25: Comparison of phase-gradient delays of SFOAEs obtained from the peak-picking algorithm for the experimentally measured data B (red crosses) and the reference (blue diamonds). The gray dashed line illustrates the whole phase-gradient of experimental data.

Finally, the measured CEOAEs were analyzed. Here, the noise present in the measurement led to too many amplitude peaks detected by the peak-picking method. Therefore, we used the Savitzky-Golay filter to smooth the CEAOE amplitude before the peak picking was applied, which led to a smaller and easily comparable number of peaks. Figure 26 illustrates that the experiment follows the reference shape, having most peak delays shorter than the expected values. The variance is larger than in Figures 24 and 25, showing SFOAE phase-gradient delays for subjects A and B.

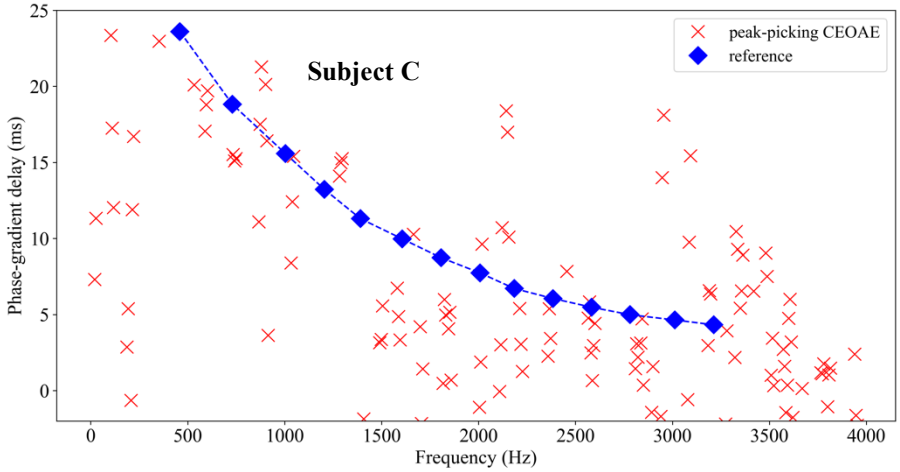

Figure 26: Comparison of phase-gradient delays of CEOAEs obtained from the peak-picking algorithm for the experimentally measured data C (red crosses) and the reference (blue diamonds).

Conclusions

This work aimed to implement and apply methods for obtaining phase-gradient delay of given reflection-source OAEs. Based on the research paper of Shera and Bergevin (2012), we have chosen the peak-picking algorithm to estimate phase-gradient delays and cepstral analysis for removing the effect of standing waves in the cochlea. Both methods were successfully implemented, and all codes are publicly available at https://github.com/josefhavlas/OAE-phase-gradient-delay.git.

We verified the mentioned methods using a nonlinear cochlear model on simulated SFOAEs and CEOAEs obtained at various stimulus intensities. With increasing intensity, the methods seem applicable for OAE latency prediction when working with the nonlinear cochlear model. Need to say that there is an inaccuracy in estimating the latencies. The analytical solution for SFOAEs derived from the cochlear model revealed that SFOAE comprises two components: one due to linear reflection (here abbreviated as CR) and the other due to perturbation of nonlinear force (here abbreviated as NL). For details see Vencovský et al. (2023). These two SFOAE components are canceling out each other. Here we show that this cancelation may result in slightly shorter latencies of the total SFOAE.

Although the peak-picking method analyzes the given data without any other change or pre-preparation of the data, it proved reliable. The method estimates the phase-gradient delays in the local maxima of OAE amplitude, and here we show that the method is reliable for various stimulus levels, especially for frequencies above about 2 kHz and for the CR component of SFOAEs.

The cepstral analysis method was shown to work properly on CEOAE data. The smoothing improved the precision at lower frequencies (approx. 1.5 kHz and lower), where only the peak-picking method predicted longer latencies due to the effect of multiple reflections of OAEs in the cochlea. On the contrary, we concluded that multiple reflections did not significantly influence our SFOAE simulations and that differences between the phase-gradient delays estimated from SFOAEs and BM transfer function are due to the natural inaccuracy of the method. In our simulations, the largest departures were visible at low frequencies (<1.5 kHz). In this case, the smoothing with the cepstral analysis did not bias the delays, which even supports the precision of the cepstral analysis method when applying it to OAEs without a big role of multiple reflections.

In addition, we applied the methods to experimentally measured SFOAEs and CEOAEs. For the SFOAE results of the peak-picking algorithm, the variation was relatively small for both subjects examined. The obtained latencies were even close to the latencies from our model, which underlines its validity. When applying the cepstral analysis method, no significant changes happened to the delays only obtained with the peak-picking algorithm.

For future research, we need to verify the methods on more data, especially on CEOAEs, where the variation is significant. We would also like to apply more methods to obtain the phase-gradient delay. Time-frequency filtering using the wavelet transform algorithm was also shown to be effective in removing additional reflections (Shera & Bergevin, 2012).

Appendix – Anatomy and physiology of hearing

This section briefly introduces the anatomical and physiological view of the human ear and heating system to better understand the otoacoustic emission generation and behavior. The description of the three ear parts was inspired by specialized literature (Maroonroge et al., 2009).

Outer ear

The human outer ear comprises two main parts – the pinna and the ear canal (see Figure 27). Its primary purpose is to attract sound waves and collect them from the outside. That is done thanks to the specific ovoid shape of the pinna, which is elastic cartilage modeled to have this ability. The ear canal is directly connected to the pinna and leads the acoustic waves to the other side of the outer ear – the tympanic membrane.

Contrary to the pinna, the ear canal is covered mainly with bone since it enters the skull, specifically the temporal bone. Only a small part (approximately the first third of its length) is protected by cartilage. Going more in the medial direction, the ear canal borders with the middle ear and leads into the tympanic membrane.

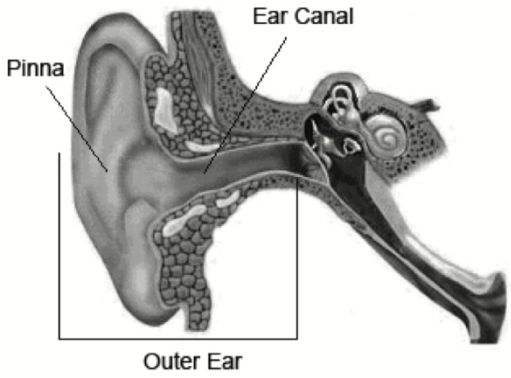

Figure 27: Outer ear. Description of outer ear parts: pinna and ear canal. Taken from (Maroonroge et al., 2009).

Middle ear

The second part of the human ear is the middle ear, a cavity located in the temporal bone (Figure 29). The tympanic membrane delimits its most external section. In the direction towards the inside of the ear, it is bordered by a bony wall. This wall isolates the middle ear from the inner one and has two windows made from a membrane – the round and oval windows.

Eardrum, called the tympanic membrane, is a cone-shaped membrane separating the outer ear's ear canal from the middle ear's cavity. Its most important function is to transmit the acoustic sound wave from the ear canal to the ossicles, which will be described later. Because of this significant functionality, its perforation or further damage can severely affect hearing ability.

The middle ear has a triplet of small bones called the malleus, incus, and stapes (see Figure 28). They are usually also called the ossicles representing all three of them together. It is fascinating that ossicles are the smallest bones in the human body, although they significantly impact our hearing.

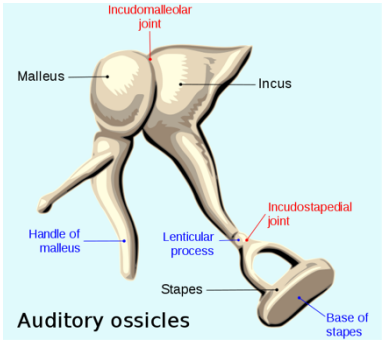

Figure 28: Detailed illustration of all three ossicles. This picture was taken from the web Wikimedia (available at: https://commons.wikimedia.org/wiki/File:Auditory_ossicles-en.svg).

Right between the middle and inner ear are two membranous windows – the round and the oval. These two structures directly connect the middle ear with the inner ear. The oval window touches the ossicular chain (consisting of all ossicles), whose principal function is to transfer sound energy from the tympanic membrane to the inner ear.

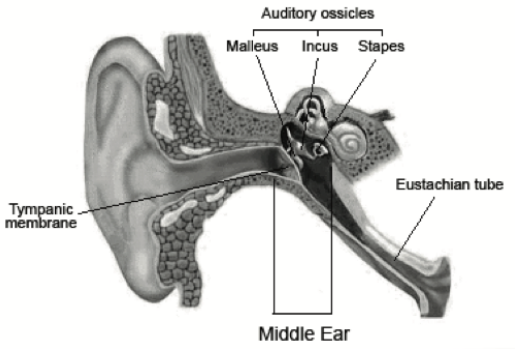

Figure 29: Overview of the middle ear. The middle ear's cavity is situated between the outer and inner ear. Here, the ossicles are essential in transferring sound waves from the outside to the inner ear. Taken from (Maroonroge et al., 2009).

The last central part of the middle ear is the Eustachian tube. It is a duct connecting the middle ear with the nasopharynx. Because the middle ear is filled with air and not directly in touch with the outer air with atmosphere air pressure, the tube works as a pressure equalizer helping the middle ear adjust to the pressure in the ear canal. The air pressure equality or significant similarity guarantees that the tympanic membrane can vibrate as much as possible after receiving an acoustic sound wave from the outside.

Inner ear

The inner ear is a significant little cavity located right next to the middle ear with which it borders. Three separate main sections can be recognized – semicircular canals, vestibule, and cochlea (Figure 30). Two structures called bony and membranous labyrinths both define the shape of the inner ear. The bony labyrinth copies the membranous one and covers it. The space between these two parts is filled with perilymph. On the contrary, the membranous labyrinth is filled with endolymph which dramatically impacts the physiology of the inner ear. The chemical characteristics of both fluids help to create an electric potential difference that maintains the physiological activities of the inner ear.

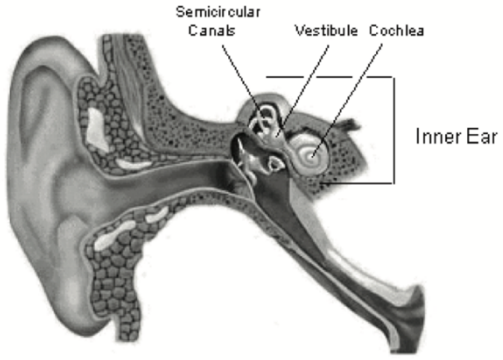

Figure 30: Unzoomed view of the human inner ear. Taken from (Maroonroge et al., 2009).

The vestibule and the semicircular canals create together the human center of balance. With the help of hair cells that they contain, they can detect the location and acceleration. This part is responsible for causing the well-known motion sickness.

The most important part, according to the topic of this thesis, is the cochlea, which is narrowly related to the generation of otoacoustic emissions (detail in Figure 31). It is formed into a snail shape in which we recognize three channels passing along the length of its curly structure (the bony spiral lamina winds up around a middle part called modiolus). These three channels are scala vestibuli, scala tympani, and scala media. Although scala media is anatomically located between the other two, mentioning them in this order is good because scala vestibuli and scala tympani are both in the bony labyrinth. On the other hand, the scala media takes part in the membranous region.

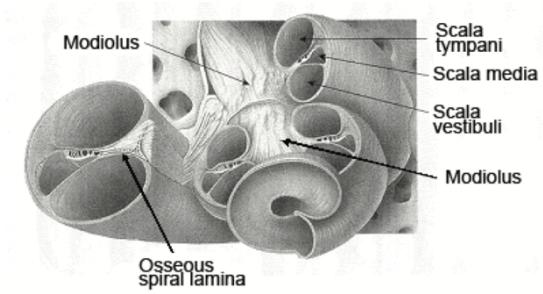

Figure 31: Cut of the human cochlea. Taken from (Maroonroge et al., 2009).

Here comes the mentioned round window separating the middle and inner ear. Its primary function is to work as a pressure valve between the bony scala vestibuli and tympani. An acoustic wave entering the hearing apparatus makes the stapes bone vibrate. This is transferred to the round window, making the perilymph in both scala vestibuli and tympani move.

We recognize a critical structure called the basilar membrane (BM) connecting scala media and tympani in the lower part of the cochlea (Figure 32). With the help of another membrane, the Reissner's, it encloses scala media into a tube-formed tunnel. It is usually slightly longer than around 30 mm aligning the whole cochlea. We divide the BM (and cochlea as well) into the base where it begins (in the direction from the middle into the inner ear) and the apex (the most central part of the coil labyrinth). The BM is thinner at the base, which causes high-frequency vibrations, and thicker at the apex, leading to vibrations at low frequencies.

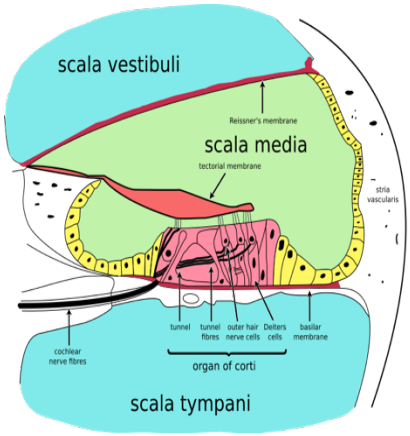

Figure 32: Detailed description of the cochlea. The bony labyrinth surrounding scala media consists of scala vestibuli and scala tympani. The basilar membrane is displayed with hair cells pointed out in the organ of Corti. From there, information is carried into the neural system. This picture was taken from Wikipedia (https://en.wikipedia.org/wiki/Cochlea.).

Cochlea hair cells

The human cochlea's basilar membrane contains the organ of Corti, the central part responsible for our hearing. This organ translates its mechanical vibrations and sends them through the vestibulocochlear nerve to the brain.

The organ of the hearing consists of two types of hair (sensory) cells that we distinguish as outer and inner. The first type is more important for us since, based on previous research and discoveries, the outer hair cells (shortly called OHCs) should be responsible for providing mechanical energy and influencing the behavior of our basilar membrane (Probst et al., 1991).

OHCs are deeply connected with hearing sensitivity which can seriously affect our daily life. They augment the BM motion depending on the location of the cells on the BM themselves. We call this phenomenon the cochlear amplifier (Young & Ng, 2023). Different frequencies stimulate hair cells. So, if they become somehow dysfunctional, it comes to the growth of sensitivity thresholds. It usually results in hearing problems. In particular, people have issues with hearing specific frequencies depending on the type of hair cells damaged (Burry, 2021).

Based on the theory of cochlear amplifier, cochlea outer hair cells are responsible for the origin of otoacoustic emissions. When observing the existence of OAEs, the performance of OHCs can be examined.

Sound waves in the hearing system

A sound is represented by an acoustical, mechanical wave traveling through the human hearing apparatus. When the pinna captures the wave, it goes through the ear canal towards the tympanic membrane. After reaching it, the eardrum vibrates and transfers this mechanical activity to the middle ear. In there, the ossicles take care of the wave transmission – the sound signal is passed through the oval window to its final destination, the inner ear. Here pressing on the oval window where it enters the coiled cochlea it forces the perilymph to ripple. These shiverings travel throughout the whole scala media's fluid until the organ of Corti. At the end of the hearing process, the vibrations are converted by hair cells into electrical energy, which makes them possible to be transmitted along the nervous system (Burry, 2021). Details of the wave traveling along the basilar membrane are shown in Figure 33.

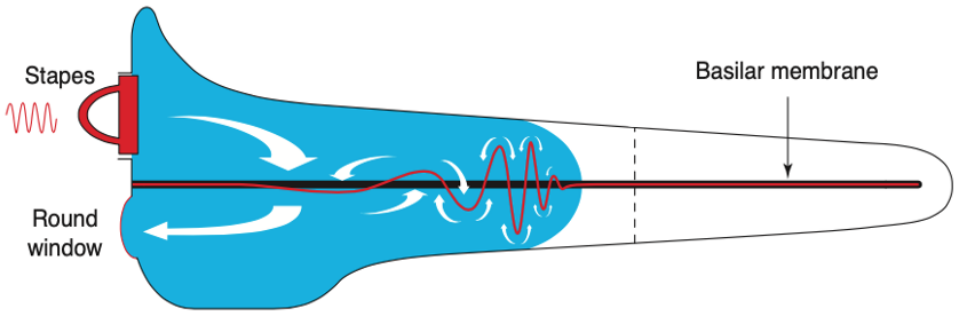

Figure 33: A traveling wave along the basilar membrane. When a sound wave leaves the middle ear, the oscillating stapes bone generates a wave that travels along the basilar membrane. At a specific point, the wave reaches its maximum and decays relatively quickly. Taken from (Nobili et al., 1998).

References

ASHA. Otoacoustic Emissions (OAEs). *American Speech-Language-Hearing Association*. Retrieved May 3, 2023, from https://www.asha.org/public/hearing/otoacoustic-emissions/

Burry, M. (2021, September 14). *How we hear: A step-by-step explanation*. Healthy Hearing. Retrieved May 4, 2023, from https://www.healthyhearing.com/report/53241-How-we-hear-explainer-hearing

Charaziak, K. K., & Shera, C. A. (2021). Reflection-Source Emissions Evoked with Clicks and Frequency Sweeps: Comparisons Across Levels. *Journal of the Association for Research in Otolaryngology : JARO*, *22*(6), 641–658. https://doi.org/10.1007/s10162-021-00813-3

Kemp, D. T. (1978). Stimulated acoustic emissions from within the human auditory system. *The Journal of the Acoustical Society of America*, *64*(5), 1386–1391. https://doi.org/10.1121/1.382104

Kemp, D. T. (2002). Otoacoustic emissions, their origin in cochlear function, and use. *British medical bulletin*, *63*, 223–241. https://doi.org/10.1093/bmb/63.1.223

Maroonroge, S., Emanuel, D. C., & Letowski, T. R. (2009). Helmet-Mounted Displays: Sensory, Perceptual, and Cognitive Issues. *USAARL*. https://www.usaarl.army.mil/assets/docs/hmds/Section-15-Chapter-8-Ear-Anatomy.pdf

Nobili, R., Mammano, F., & Ashmore, J. (1998). How well do we understand the cochlea?. *Trends in neurosciences*, *21*(4), 159–167. https://doi.org/10.1016/s0166-2236(97)01192-2

Probst, R., Lonsbury-Martin, B. L., & Martin, G. K. (1991). A review of otoacoustic emissions. *The Journal of the Acoustical Society of America*, *89*(5), 2027–2067. https://doi.org/10.1121/1.400897

Shera, C. A., & Bergevin, C. (2012). Obtaining reliable phase-gradient delays from otoacoustic emission data. *The Journal of the Acoustical Society of America*, *132*(2), 927–943. https://doi.org/10.1121/1.4730916

Shera, C. A., & Charaziak, K. K. (2019). Cochlear Frequency Tuning and Otoacoustic Emissions. *Cold Spring Harbor perspectives in medicine*, *9*(2), a033498. https://doi.org/10.1101/cshperspect.a033498

Shera, C. A., & Guinan, J. J., Jr (1999). Evoked otoacoustic emissions arise by two fundamentally different mechanisms: a taxonomy for mammalian OAEs. *The Journal of the Acoustical Society of America*, *105*(2 Pt 1), 782–798. https://doi.org/10.1121/1.426948

Shera, C. A., & Guinan, J. J., Jr (2003). Stimulus-frequency-emission group delay: a test of coherent reflection filtering and a window on cochlear tuning. *The Journal of the Acoustical Society of America*, *113*(5), 2762–2772. https://doi.org/10.1121/1.1557211

Shera, C. A., & Guinan, J. J., Jr. (2008). Mechanisms of Mammalian Otoacoustic Emission. In: Manley, G.A., Fay, R.R., Popper, A.N. (eds) *Active Processes and Otoacoustic Emissions in Hearing*. Springer Handbook of Auditory Research, vol 30. Springer, New York, NY. https://doi.org/10.1007/978-0-387-71469-1_9

Shera, C. A., Guinan, J. J., Jr, & Oxenham, A. J. (2010). Otoacoustic estimation of cochlear tuning: validation in the chinchilla. *Journal of the Association for Research in Otolaryngology : JARO*, *11*(3), 343–365. https://doi.org/10.1007/s10162-010-0217-4

Shera, C. A., & Zweig, G. (1993). Noninvasive measurement of the cochlear traveling-wave ratio. *The Journal of the Acoustical Society of America*, *93*(6), 3333–3352. https://doi.org/10.1121/1.405717

Talmadge, C. L., Long, G. R., Murphy, W. J., & Tubis, A. (1993). New off-line method for detecting spontaneous otoacoustic emissions in human subjects. *Hearing research*, *71*(1-2), 170–182. https://doi.org/10.1016/0378-5955(93)90032-v

Vencovský, V., Klimeš, O., & Vetešník, A. (2023). A Component of Stimulus-Frequency Otoacoustic Emissions Evoked due to Perturbation of Nonlinear Force in a Cochlear Model. *Conference Proceeding,s Mechanics of Hearing Workshop.* [in press].

Vetešník, A., Vencovský, V., & Gummer, A. W. (2022). An additional source of distortion-product otoacoustic emissions from perturbation of nonlinear force by reflection from inhomogeneities. *The Journal of the Acoustical Society of America*, *152*(3), 1660. https://doi.org/10.1121/10.0013992

Young, A., & Ng, M. (2023). Otoacoustic Emissions. *StatPearls Publishing*. https://www.ncbi.nlm.nih.gov/books/NBK580483/